NASA CR-165214
EDA 201-3A

FINITE ELEMENT FOR ROTOR/STATOR INTERACTIVE FORCES IN GENERAL ENGINE DYNAMIC SIMULATION

PART I: DEVELOPMENT OF BEARING DAMPER ELEMENT

M. L. Adams
J. Padovan
D. G. Fertis

October 1980

Department of Civil Engineering
Department of Mechanical Engineering
The University of Akron
Akron, Ohio 44325

Prepared for
LEWIS RESEARCH CENTER
NATIONAL AERONAUTICS AND SPACE ADMINISTRATION
CLEVELAND, OHIO 44135

NASA Grant NSG 3283

1. Report No.	2. Government Accession No.	3. Recipient's Catalog No.
NASA CR-165214		

4. Title and Subtitle	5. Report Date
Finite Element for Rotor/Stator Interactive Forces in General Engine Dynamics Simulation, Part I: Development of Bearing Damper Element	October 1980
	6. Performing Organization Code

7. Author(s)	8. Performing Organization Report No.
M. L. Adams, J. Padovan, D. G. Fertis	
	10. Work Unit No.

9. Performing Organization Name and Address	11. Contract or Grant No.
Department of Mechanical Engineering The University of Akron Akron, OH 44325	NSG-3283
	13. Type of Report and Period Covered
12. Sponsoring Agency Name and Address	Topical
National Aeronautics and Space Administration Washington, DC 20546	14. Sponsoring Agency Code

15. Supplementary Notes

Technical Monitor: C. C. Chamis, M.S. 49-6
NASA Lewis Research Center
21000 Brookpark Road
Cleveland, OH 44135

16. Abstract

A general purpose squeeze-film damper interactive force element has been developed, coded into a software package (module) and debugged. This software package has been applied to nonlinear dynamic analyses of some simple rotor systems. Results for pressure distributions show that the long-bearing (end-sealed) is a stronger bearing as compared to the short-bearing as expected. Results of the nonlinear dynamic analysis, using a four-degree-of-freedom simulation model, showed that the orbit of the rotating shaft increases nonlinearly to fill the bearing clearance as the unbalanced weight increases.

17. Key Words (Suggested by Author(s))	18. Distribution Statement
Nonlinear analysis, squeeze film dampers, bearings, aircraft engines, nonlinear dynamics, structural dynamics, finite element, Reynold's equation, shaft orbits.	Unclassified, Unlimited

19. Security Classif. (of this report)	20. Security Classif. (of this page)	21. No. of Pages	22. Price*
Unclassified	Unclassified		

* For sale by the National Technical Information Service, Springfield, Virginia 22161

FORWARD

This report presents the work performed under NASA Grant NSG-3283, August 1, 1979 to July 31, 1980, with Dr. C. C. Chamis, NASA Lewis Research Center as Project Manager. It is the first in a series of reports on the development of rotor/stator interactive force elements for implant into general purpose nonlinear time-transient finite-element codes suitable for general engine dynamic simulation. The Principal Investigators on this grant were Drs. M. L. Adams, J. Padovan and D. G. Fertis of the University of Akron. Mr. Ibrahim F. Zeid, doctoral student at the University of Akron, has also contributed heavily in this effort.

NOMENCLATURE

C = radial clearance of damper annulus

D = nominal damper annulus diameter = $2R$

e = damper eccentricity

F_x = X - component of damper force

F_y = Y - component of damper force

h = damper annulus film thickness distribution

L = damper length

p = damper film thickness distribution

R = nominal damper annulus radius

t = time

x = $R\theta$ = damper annulus circumferential coordinate

X = X - direction radial motion coordinate

Y = Y - direction radial motion coordinate

z = damper annulus axial coordinate

μ = damper lubricant viscosity

Ω = frequency of vibration excitation

SPECIAL TERMINOLOGY

Infinitely Long Bearing Model - axial flow is neglected ($\frac{\partial}{\partial z} << \frac{\partial}{\partial x}$)

Infinitely Short Bearing Model - circumferential flow is neglected ($\frac{\partial}{\partial x} << \frac{\partial}{\partial z}$)

Driver Code - Any computer code which calls the squeeze-film damper force computation code

TABLE OF CONTENTS

Section 1

SUMMARY

As a result of the first-year effort on this grant, a general purpose squeeze-film damper interactive force element has been developed, coded and debugged. This software package has been applied in nonlinear dynamic analyses of some simple rotor systems.

The work completed under this first-year grant is a significant step in the development of strategies and add-on software packages which will be needed to apply available advanced nonlinear finite-element codes (such as ADINA) to general engine dynamic simulation. Also, a detailed discussion is provided of the direction of effort for the next two years.

Section 2

INTRODUCTION AND BACKGROUND

2.1 Engine System Dynamics

Present day jet engine configurations have evolved primarily through a trial-and-error process involving extensive testing. There are many fundamental dynamic phenomena which take place within these engines for which basic description and understanding have yet to be generated. Nonetheless, they work well. Modern aircraft engines are typical of current high-technology products in which the recently acquired computing capabilities of today are being used to better understand and improve what is already designed, built and operating.

A better understanding of the basic dynamic characteristics of existing and new engine configurations is a prerequisite for producing acceptable engine efficiencies on advanced configurations (i.e. smaller rotor/stator running clearances). Also, a better definition of engine dynamic response would more than likely provide valuable information leading to reduced maintenance and overhaul costs on existing configurations. Furthermore, application of advanced engine dynamic simulation methods could potentially provide a considerable cost reduction in the development of new engine configurations by eliminating some of the trial-and-error process done with engine hardware.

The emergence of advanced finite element codes, such as NASTRAN, NONSAP, MARC and ADINA, and related algorithmic advances, have placed comprehensive engine system dynamic analyses within

reasonable reach. What remains to be done is to develop new component element software to properly model engine rotor/stator interactive components, such as squeeze-film damper, within the algorithmic logic of already proven finite element codes. This is the major mission of this grant.

2.2 The Function of Squeeze-Film Dampers

For good reasons, aircraft engines use rolling element bearings exclusively. This design philosophy has, until recent years, deprived engines of the beneficial damping inherent in many other types of rotating machinery where fluid-film journal bearings are used. The implementation of squeeze-film dampers in recent engine designs has now provided engine designers with an effective means of vibration energy dissipation. The net result is that the newer engines with squeeze-film dampers are less sensitive to residual rotor imbalance and better able to control vibration and transmitted force levels resulting from various excitation sources within the engine.

2.3 Currently Available Analysis Procedures and Limitations

The field of rotor dynamics has evolved to its present state primarily through the solution to problems in types of machinery other than aircraft engines. In most other types of rotating machinery (e.g., steam turbines, centrifugal pumps and compressors, fans, generators, motors, etc.) the rotor can be adequately modelled as an Euler or Timoshenko beam.[1] In addition, the support structure holding each bearing can often be adequately modelled as a separate mass-damping-stiffness path to ground

(i.e., to the inertial frame). Also, for most purposes, bearing lubricating film dynamic properties are characterized as stiffness and damping elements, linearized for small vibration amplitudes about some static equilibrium state. It is this level of sophistication that has been utilized for the most part in rotor-dynamic analyses of aircraft engines (e.g., Hibner [2]).

Present day aircraft engines are structurally far more complex than most other types of rotating machinery. The multi-shaft configuration, plus the fact that the shafts are thin rotating shells, not simple beams, creates unique but significant complicating differences between aircraft engines and other machinery. Also, the stator structural support at each rotor bearing represents anything but a separate mass-damper-stiffness path to an inertial frame. In fact, setting the inertial frame for the engine is not a simple matter when the full range of in-service maneuvers is realized. Dynamic paths between different bearings exist not only through the rotor but through several other paths within the non-rotating engine structure, i.e., a "multi-level multi-branch" system. As many as eight significant "levels" have been identified.

The feasibility of nonlinear dynamic analyses of multi-bearing flexible rotors has been recently demonstrated on non-aircraft applications (see Adams [3]). There are highly non-linear dynamic effects in aircraft engines, particularly under large excitation forces, such as blade or disk failures, hard landings and foreign matter ingestion events.

Clearly, the field of aircraft engine dynamics is presently in a position where there is both a need for substantial advances and feasible means available by which such advances can be accomplished.

2.4 The Need for Time-Transient Nonlinear Dynamic Analyses

In recent years it has become evident that an important class of engine dynamic phenomena can not be studied without accounting for the highly nonlinear forces produced at bearings, labyrinths and other close-running rotor/stator clearances under large amplitude vibrations. In such cases, linear theory typically predicts vibration amplitudes larger than the actual running clearances. Furthermore, important vibratory phenomena, such as subharmonic resonance and motion limit cycles, are "filtered" out of the problem with a linear model, giving grossly erroneous predictions, qualitatively as well as quantitatively.

With few exceptions, nonlinear dynamic problems must be solved numerically as time-transient responses, whether the sought "answer" is a steady state periodic motion or is strictly a transient phenomenon. The problem is mathematically categorized as an initial value problem in which the displacements and velocities of the complete system must all be specified at the beginning of the transient. From that point forward in time, the equations of motion are numerically integrated (known as "marching") as far in time as one wishes to study the system motions and forces. If the system is dynamically stable, the transient motion dies out yielding the steady state response

which in a system with a periodic force excitation will be a periodic motion. In a stable system with no time-varying force excitation, the transient will die out as the system comes to rest at one of its stable static equilibrium positions. If the system is unstable, the transient does not die out but continues to grow in time unless or until some nonlinear mechanism in the system limits the motion to what is frequently called a "limit cycle".

In order to study the general dynamical characteristics of aircraft engines, nonlinear dynamic computational schemes are required. The approach taken in this grant is to develop software packages to model engine components which are not typically found on dynamical structures and therefore are not already built into existing nonlinear finite-element structural dynamics computer codes. This first-year effort has concentrated on developing such a software package for squeeze-film bearing dampers.

2.5 First-Year Effort, Development of Damper Element

The main objective of the first-year effort was to develop a squeeze-film damper element (i.e., software package) suitable for implant into a general purpose nonlinear finite-element computer code. This objective has been met in full. Furthermore, workable strategies have already been developed to implant this damper element. Also, the damper element has been extensively tested on simple rotor/stator configurations under a wide variety of dynamic loading conditions. These results are presented in subsequent sections of this report.

Section 3

BEARING DAMPER ELEMENT

3.1 Introduction

The bearing damper finite element code is essentially an interactive element to represent squeeze film dampers. That is, its purpose is to bridge the "gap" between structural elements which are separated in the actual engine by a squeeze film damper. In its simplest version, it has an input/output setup as shown in Figure 1. As the bearing-damper element is extended to encompass more types of rotor/stator interactive forces (e.g., rubs, impacts, etc.) the input/output list will expand.

A source listing of the bearing damper element code developed during the first-year is given in Appendix A of this report.

3.2 Governing Equations

The rotor/stator interactive force generated in a bearing squeeze film damper is modeled using an adaptation of the classical Reynolds lubrication equation for incompressible laminar isoviscous films.

$$\frac{\partial}{\partial x}\left(\frac{h^3}{\mu}\frac{\partial p}{\partial x}\right) + \frac{\partial}{\partial z}\left(\frac{h^3}{\mu}\frac{\partial p}{\partial z}\right) = 6\frac{\partial}{\partial x}(hU) + 12\frac{dh}{dt} \qquad (1)$$

z = axial coordinate

x = circumferential coordinate = $r\theta$

h = local film thickness

$\frac{dh}{dt}$ = instantaneous local rate of change in h

U = sliding velocity = $R\omega$, typically zero in a damper

C = radial clearance of damper annulus

The relationship between system inertial coordinates and damper parameters comes through the expression for h, $\partial h/\partial x$ and dh/dt. Referring to Figure 2, these relationships are summarized as follows:

$$\bar{e} = (X_R - X_S)\hat{i} + (Y_R - Y_S)\hat{j} \tag{2}$$

$$\dot{\bar{e}} = (\dot{X}_R - \dot{X}_S)\hat{i} + (\dot{Y}_R - \dot{Y}_S)\hat{j} \tag{3}$$

then

$$h = C - \bar{e}\cdot\hat{n}_\theta = C - (X_R - X_S)\cos\theta - (Y_R - Y_S)\sin\theta \tag{4}$$

$$\frac{\partial h}{\partial x} = \frac{1}{R}\frac{\partial h}{\partial \theta} = \frac{1}{R}\left[(X_R - X_S)\sin\theta - (Y_R - Y_S)\cos\theta\right] \tag{5}$$

and

$$\frac{dh}{dt} = -(\dot{X}_R - \dot{X}_S)\cos\theta - (\dot{Y}_R - \dot{Y}_S)\sin\theta \tag{6}$$

3.3 Typical Configurations and Boundary Conditions (see Figures 3,4,5)

Some engine manufacturers do not use centering springs in general on either military or commercial application because of fatigue. This can require using a tighter clearance and thus requires a tighter control on dimensional tolerances on annulus diameters. In both cases $\frac{\partial p}{\partial z} << \frac{\partial p}{\partial x}$, i.e., axial pressure drop within annulus is much smaller than circumferential pressure drop. This reduces the governing equation (1) to,

$$\frac{d}{dx}\left(\frac{h^3}{\mu}\frac{dp}{dx}\right) = 12\frac{dh}{dt} \tag{7}$$

the "infinitely long" bearing equation for zero rotation (U = 0).

Other less frequently used configurations do not employ end seals, in which case the "short bearing" approximation or its equivalent is used. In this case, the local axial end flow is considered to far outweigh the circumferential flow leading the "short bearing" approximation.

$$\frac{d}{dz}\left(\frac{h^3}{\mu}\frac{dp}{dz}\right) = 12\frac{dh}{dt} \tag{8}$$

Actually, an improved adaptation of the short-bearing approach is obtained by implementing the parabolic assumption of O'Donoghue [9]. That is, the following approximation is made,

$$p(\theta,z) = p(\theta,0)\left(1 - \frac{4z^2}{L^2}\right) \tag{9}$$

which assumes an axially symmetric axial pressure distribution at every circumferential location. This then gives the following pressure field equation.

$$\frac{1}{\mu}\frac{\partial}{\partial x}\left(h^3\frac{\partial p}{\partial x}\right) = 12\frac{dh}{dt} + 8\frac{p(\theta,0)h^3}{L^2} \tag{10}$$

This is actually a first-order Fourier approximation using the parabola as the single approximative function.

A convergent approximation to the full two-dimensional Reynolds equation can be obtained, as an extension of the foregoing approach by O'Donoghue [9]. The number of Fourier terms is increased to N, resulting in N simultaneous ordinary differential equations.

$$p(\theta,z) = p_1(\theta,0)\cos\frac{\pi z}{L} + p_2(\theta,0)\cos\frac{3\pi z}{L} + \ldots + p_N(\theta,0)\cos\frac{(2n-1)\pi z}{L} \tag{11}$$

Substitution into the general 2-D Reynolds equation (1), expansion of the right hand side (RHS) by the same series, followed by LHR:RHS segregation by the arguments under cosine yields N ordinary differential equations, one for each $p_i(\theta,0)$.

3.4 Method of Solution

Whether the long-bearing formulation (7) or the other two formulations described by (10) and (11) are used, the following solution method is employed. It is described below as implemented for the long-bearing formulation.

Based on 3-point central difference,

$$h^3 \frac{d^2p}{dx^2} + 3h^2 \frac{dh}{dx}\frac{dp}{dx} = 12\mu \frac{dh}{dt}$$

$$\left(\frac{dp}{dx}\right)_i = \frac{P_{i+1} - P_{i-1}}{2\Delta x}$$

$$\left(\frac{d^2p}{dx^2}\right)_i = \frac{P_{i+1} - 2P_i + P_{i-1}}{\Delta x^2}$$

$$h_i^3 \left(\frac{P_{i+1} - 2P_i + P_{i-1}}{\Delta x^2}\right) + 3h_i^2 \frac{dh_i}{dx}\left(\frac{P_{i+1} - P_{i-1}}{2\Delta x}\right) = 12\mu \frac{dh_i}{dt} \qquad (12)$$

Rearranging

$$P_{i+1}\underbrace{\left[\frac{h_i^3}{\Delta x^2} + \frac{3h_i^2}{2\Delta x}\frac{dh_i}{dx}\right]}_{D_j} + P_i\underbrace{\left[-\frac{2h_i^3}{\Delta x^2}\right]}_{C_j} + P_{i-1}\underbrace{\left[\frac{h_i^3}{\Delta x^2} - \frac{3h_i^2}{2\Delta x}\frac{dh_i}{dx}\right]}_{E_j} = \underbrace{12\mu \frac{dh_i}{dt}}_{R_j}$$

Recurrsion relationship,

$C_jP_j + E_jP_{j-1} + D_jP_{j+1} = R_j$, form of difference equation

Employ the form,

$$P_{j-1} = A_j P_j + B_j$$

Then,

$$C_j P_j + E_j(A_j P_j + B_j) + D_j P_{j+1} = R_j$$

or

$$P_j(C_j + E_j A_j) + E_j B_j + D_j P_{j+1} = R_j$$

Then,

$$P_j = \left(\frac{-D_j}{C_j + E_j A_j}\right) P_{j+1} + \frac{R_j - E_j B_j}{C_j + E_j A_j}$$

$$A_{j+1} = -\frac{D_j}{C_j + E_j A_j}$$

$$B_{j+1} = \frac{R_j - E_j B_j}{C_j + E_j A_j} \qquad (13)$$

From upstream boundary condition the {A} and {B} vectors are determined by starting with $A_2 = 0$, $B_2 = P_1$ (called forward sweep).

The downstream boundary condition is inserted at the beginning of the backward sweep, i.e.

$$P_{M-1} = A_M P_M + B_M$$

$$P_{M-2} = A_{M-1} P_{M-1} + B_{M-1}$$

$$\vdots \qquad \vdots$$

$$P_2 = A_3 P_3 + B_3$$

Film rupture is handled by the following substitution. If $P_j < P_{vapor}$, set $P_j = P_{vapor}$ before computing p_{j-1}. This is

equivalent to the condition $\frac{\partial p}{\partial x} = 0$ at the film-rupture full-film boundary. In the case of the 2-D convergent approach indicated by eqn. (11), this point-by-point test is made on the local summation $P(\theta_j,z) = \sum_{k=1}^{N} P_k(\theta_j,z)$.

The method of solution although not closed-form, is non-iterative. While it does entail a one-dimensional finite-difference scheme, it requires only a very small amount of CPU time and is therefore ideally suited to time transient rotor dynamics analyses. It has major advantages over the purely closed-form approximations, e.g., [10,11]. These major advantages are immediate account of specified-pressure boundary conditions at feed and drain holes of a damper. Also, the finite difference approach easily permits account of static as well as dynamic deflections which alter the oil film gap geometry from ideal rigid circular shapes.

3.5 Force and Force Gradients

Forces Components on Rotor:

$$F_X = -\int_A p \cos\theta dA = -LR\int_{\theta_1}^{\theta_2} p(\theta)\cos\theta d\theta$$
$$F_Y = -\int_A p \sin\theta dA = -LR\int_{\theta_1}^{\theta_2} p(\theta)\sin\theta d\theta \qquad (14)$$

Stator Force Components:

$$F'_X = -F_Y \ , \quad F'_Y = -F_Y \qquad (15)$$

Force Gradients:

$$[C_{ij}]_{2x2} = -\frac{\partial F_i}{\partial \dot{X}_j} \ ; \quad [K_{ij}]_{2x2} = -\frac{\partial F_i}{\partial X_j}$$
$$\frac{\partial F_i}{\partial \dot{X}_j} \simeq \frac{\Delta F_i}{\Delta \dot{X}_j} \ ; \quad \frac{\partial F_i}{\partial X_j} \simeq \frac{\Delta F_i}{\Delta X_j} \qquad (16)$$

Numerical differentiation is performed with small $\Delta\dot{X}_j$ and ΔX_j increments about instantaneous conditions. This provides continuous updating of $\{F_j\}$, $[C_{ij}]$ and $[K_{ij}]$. See Appendix A for the computer code source listing of the completed squeeze-film element SQUEEZ.

Section 4
APPLICATION OF DAMPER ELEMENT

4.1 Introduction

For purposes of checking out the damper element code and to demonstrate its use, two types of computations were made and the results presented herein. First, a parametric study of damper pressure distributions was made for a variety of specified circular orbits, for both long-bearing and short bearing solutions. Second, a four-degree-of-freedom rotor-damper-stator model was investigated under conditions of small rotor unbalance through large rotor unbalance. These results are reported in the following sections.

4.2 Pressure Distributions for Specified Circular Orbits

For this series of computations the following damper annulus parameters were used.

Diameter, D = 6 in.

Length, L = 1.25 in.

Radial clearance, C = 0.010 in.

Lubricant viscosity, $\mu = 1 \times 10^{-6}$ reyns

Angle between inlet oil port and drain port, $(\theta_i - \theta_o) = 180°$

Inlet oil port pressure, P_i = 55 psia

Drain port pressure, p_o = 15 psia

Lubricant vapor pressure, p_v = 1.5 psia

Orbit angular velocity, Ω = 3600 cpm (376.99 rad/sec)

The above damper parameters are typical for modern gas turbine aircraft engines. A parametric study was made postulating the outer ring of the damper fixed and the inner ring having a constant-radius constant-velocity concentric orbit. Eccentricity ratios (i.e., orbit radius/radial clearance) from 0.05 to 0.95 were computed, both for the long-bearing and short-bearing solutions (both are presently incorporated in the damper-element computer code).

Circumferential center-line pressures were plotted as a function of circumferential position and time, for one period of prescribed motion. The results for the long-bearing solution are shown in Figure 6, and Figure 7 for the short-bearing solution. The difference between long-bearing and short-bearing solutions is quite large, particularly as motion amplitudes get smaller. The long-bearing solution provides a considerably stronger damper, thus the common preference of designers to use end-sealed dampers.

4.3 Nonlinear Dynamic Response of Simple Rotor Systems

A simple "driver" code was written (see Appendix B for listing) which uses the damper-element code in the same manner as a general application with large finite-element codes. The "driver" code is based on a four (4) degree-of-freedom system

i.e., planar motion of the inner and outer damper elements. This then simulates a single-mass rotor connected to a single-mass stator via the damper element. The system analyzed is shown in Figure 8. The model is coded to simulate arbitrary rotating and/or static radial loads. Aside from demonstration purposes, this four (4) degree-of-freedom model has been devised to check against the same type of system when executed with the damper element implanted into the general purpose nonlinear finite-element code ADINA, which the University of Akron has purchased as its contribution to this grant.

Note from Figure 8 that the high pressure port (i.e., feed port) is located on the bottom of the damper so as to assist "lift-off". Since centering springs are not typically used, they have been excluded in this example. Lift-off therefore requires some amount of vibration to overcome the dead weight load. Rotating unbalance loads of 100, 200, 300, 500 and 1000 lbs were run with Ω = 150 rad/sec. Orbital plots were made showing rotor and stator total motion on one plot and rotor-relative-to-stator motion on a second plot. The plotted results are shown in Figure 9 through 13.

For a 100 lb rotating load (Figure 9) the motions shown are for a 20 cycle transient from time = 0. The rotor and stator each show close to the same motion, and their relative motion is small, with the rotor barely "lifting off". The relative orbit is essentially oscillatory. However, when the rotating load is increased to 200 lbs, (Figure 10), the relative orbital

motion shows the beginnings of orbital motion, i.e., a "cresent moon" shape as measured by numerous investigators. Further increase in magnitude of the rotating load to 300 lbs (Figure 11) shows a well defined steady-state total motion as well as relative motion. Note that with a 300 lbs rotating load, the relative (rotor-to-stator) orbit is still small in comparison to the radial damper clearance and confined to the region of the bottom of the damper. However, an increase of rotating load magnitude to 500 lbs causes a considerable change to the relative orbit (Figure 12). Notice now that the relative motion of the rotor with respect to the stator fills a major portion of the clearance circle. Further increase of rotating load magnitude to 1000 lbs (Figure 13) simply causes the steady-state relative orbit to expand and fill even more of the damper clearance circle.

Section 5
FINITE ELEMENT IMPLANT STRATEGY

The previous sections gave a thorough discussion of the development of the interactive squeeze film bearing element. This section will outline ongoing efforts aimed at incorporating these elements into the finite element procedure. In this context, the discussion will be organized into several main parts, namely:

i) Choice of FE code used for initial implantation;
ii) Overall solution strategy; and,
iii) Solution algorithms employed.

5.1 Choice of FE Code Used for Initial Implantation

Before discussing the choice of FE code adopted, it is worthwhile to briefly overview various of the salient features associated with rotor-bearing-stator modelling. To organize our thoughts, we consider them in two main phases, namely:

i) Normal operating conditions; and,

ii) Abnormal operating conditions.

For normal situations, since the clearance between the blade and shroud and the various engine seals are quite small, the overall kinematic description can be characterized by small strains superposed on an initially small field [4]. Because of this, except for local zones, the overall structural material characterization can be considered essentially Hookean in nature. In this context, the structural modelling of the engine can be considered essentially linear in nature. Regardless of this though, as has been seen from the discussion in the previous sections, even small unbalance loads can initiate highly nonlinear interactive forces in the squeeze film bearings. Because of such nonlinearity, under normal operating conditions the rotor-bearing-stator system can be modelled as a partitioned system wherein the structural components are linear while the bearings are nonlinear.

For abnormal operating conditions, the rotor excursions are on the order of the various blade and seal clearances. In this context, due to the relative smallness of such clearances, the deformation process can be characterized by at most small

strain moderate rotations superposed on small initial fields [12]. Since such kinematic excursions are still deemed small, except for local events *, the global structural material behavior can still be considered Hookean. Because of this, the structural modelling of the engine can be assumed kinematically nonlinear. Obviously, during a fatal event both kinematic and massive material nonlinearity are evidenced during structural collapse.

In the context of the foregoing, it is of utmost importance that the FE test code chosen have adequate nonlinear element substructural capabilities to allow for the proper partitioning into linear and nonlinear element groups. This obviously enables more efficient running characteristics. Together with the partitioning capabilities, the code should also have an efficient updating architecture. As this feature is typically the heart of any nonlinear solution strategy, it is an absolutely essential characteristic. In addition to the foregoing features, the code chosen to test the bearing element should have [5]:

i) Accessible program architecture;
ii) Efficient running characteristics; and,
iii) Flexible algorithmic options.

---

* blade impacts, creep/fracture of blades

Since many general purpose codes such as NASTRAN, STRUDL, FESAP, etc. are essentially linear with grafted nonlinear capabilities, they tend to have a less efficient/flexible program architecture. Because of this, our attention must turn to codes such as ADINA, ANSYS, MARC, etc. Since ANSYS and MARC have somewhat inaccessible program architecture, the ADINA program was chosen to check out the "bearing element implant". This follows since ADINA has the requisite combinations of capabilities, namely [6].

i) Nonlinear element partitioning feature;
ii) Efficient updating architecture;
iii) Flexible algorithmic options;
iv) Accessible program architecture; and,
v) Efficient running characteristics.

5.2 Overall Solution Strategy

The initial approach taken has been to implant the bearing element directly into the ADINA architecture so that direct numerical time integration algorithms can be employed to generate the transient rotor stator solution. To simplify the discussion, the presentation will be organized into several main areas, namely:

i) Element architecture;
ii) Overall FE code architecture; and,
iii) Solution methology

The overall architecture of the bearing element is being structured to have several main options, namely:

i) Initial I/O;

ii) Interactive I/O;

iii) Generalized stiffness and damping connectivity; and,

iv) Generalized element library.

The initial I/O options involve a one-time input of various pre-selected parameters including such categories as:

i) Geometric configuration;

ii) Material properties;

iii) Element selection; and,

iv) Required element connectivities.

Each of these categories are in turn broken down into several different items, for instance:

1. Geometric Configuration

   i) Inner and outer damper radii

   ii) Bearing length

   iii) Orientation of oil feed grooves

   iv) Structural clearances

   v) Placement of roller bearings

2. Material Properties

   i) Oil properties

   ii) Temperature dependence

   iii) Roller bearing force deflection characteristics

3. Element Selection

   i) Short bearing

   ii) Infinite bearing

   iii) Roller bearing characterization

   iv) Rub/impact

4. Required Element Connectivities

Several of the foregoing parameters are being coded to be interactively redefined depending on the nature and level of excitation for example, temperature and structural clearances fall into this category. Additionally, such field variables as film forces as well as the instantaneous tangent stiffness and damping matrices are being coded so as to be interactively redefined. Such parameters are up dated depending on the nature of the interactively calculated position and velocity histories. In this context, the various interactive field quantities now being coded into the bearing implant associated with the ADINA code consist of:

1. Velocity differential developed across the squeeze film;
2. Positional differential developed across the squeeze film;
3. Interactive force field developed;
4. Tangent stiffness matrix developed by suqeeze film;
5. Tangent damping matrix developed by squeeze film; and,
6. Tangent stiffness of roller bearing.

To generalize the capability of the "bearing implant", the initial and interactive I/O modes of data transfer are being developed so as to admit fairly extensive structural con-

figurations. This includes the possibility of accessing the entire array of structural elements inherent to ADINA together with the various constitutive models including

1. Hookean
2. Plasticity
3. Temperature dependent properties
4. Mooney Rivilin [3], etc.

The overall architecture of the bearing implant is defined in Figures 14 and 15. As can be seen in Figure 14, the bearing implant is being imbedded in a buffer routine which will serve primarily as a link between the various data transfer modes of ADINA, namely:

i) Common blocking (dynamic form);
ii) Subroutine parameter lists;
iii) Disk I/O.

The buffer routine will also serve to convert the interactive information into the appropriate partitioned form for assembly into the mainstream of data flow inherent to ADINA. Namely, the tangent stiffness and damping matrices together with the interactive forces will be assembled into the proper locations in their global counterparts. This is currently being programmed into both the in core and out of core storage mode options inherent to ADINA.

Additionally, the buffer routine will be programmed to contain a degree of adaptive updating which will enable a more accurate calculation of the tangent stiffness and damping matrices.

Specifically, since the stiffness and damping matrices are calculated by admitting a perturbation in the position and velocity fields of a given state, care must be taken to insure that the perturbation is neither too small nor too large. In the case that the perturbation is too large then the stiffness calculated will act more like a secant stiffness and hence be inaccurate. If too small, then roundoff error may be introduced into the calculations. To circumvent this difficulty, the current and past fields are compared. If the percentage changes are deemed too large/small, then the levels of perturbation introduced can be either contracted or expanded to insure proper evaluation of the tangent matrices.

While the structure of the buffer will be somewhat dependent on the ADINA architecture [7] the main core of the beam implant will be more or less code independent. The actual flow of data into the core of the implant is achieved by subroutine argument lists. Figure 15 defines the overall flow of control within the core program of the bearing implant. The architecture of the core program is being made flexible enough to admit new options as they become available.

Based on the foregoing bearing element implant, the architecture of the overall FE code is defined in Figure 16. As can be seen, the overall flow of control is broken into several major steps, namely:

1. Initial I/O, including:
   i) Structural information
   ii) Bearing information

iii) Boundary conditions

iv) Applied load

v) Element connectivities

2. Structural element generation, including:

i) Linear elements

ii) Partitioned assembly of linear elements

iii) Nonlinear stiffness update loop with partitioned assembly of nonlinear structural elements

3. Bearing element generation, including:

i) Tangent stiffness and damping matrix generation

ii) Development of right-hand side loads

iii) Partitioned assembly

4. External load generation

5. Integration algorithm, including:

i) "Stiffness" inversion

ii) Implicit integration

a) Newmark

b) Wilson

iii) Explicit integration

a) Central difference

6. Convergence checks

i) Norm test of out of balance loads and nodal displacements

ii) Higher order checks

7. Clearance checks

8. Adaptive Strategies, including [7]:

   i) Structural stiffness updating

   ii) Bearing stiffness updating

   iii) Choice of perturbation size

   iv) Choice of integration algorithm

   v) Choice of time step size

   vi) Preferential partitioned updating, etc.

A simplified view of the actual flow of control is given in Figure 17. This figure includes both the linear and nonlinear structural loops. Currently such modifications are being inserted into the ADINA architecture.

5.3 Solution Algorithms

As noted earlier, having developed the "bearing element", the current thrust is to implant the element into ADINA wherein direct numerical integration will be employed to generate the transient solution. In this context, several types of integration operators are being incorporated into the coding. In particular various versions of the following operators are being considered:

1. Newmark [9]
2. Wilson [10]
3. Houbolt [11]
4. Central difference [11]
5. Hughes [12]
6. Felippa, Park, etc. [13]

Section 6
DISCUSSION - DIRECTIONS OF FUTURE WORK

In view of the modelling deficiencies noted earlier, a more direct way of handling the structural aspects of the rotor-bearing-support (RBS) system is necessary if a proper transient/steady state model is to be developed for jet engines. In this direction, it appears that the finite element (FE) method is the requisite modelling approach for such problems. This follows from the fact that its inherent capabilities include the following features:

i) The FE procedure has the capability to handle multi-branch/level structure in a more direct and efficient manner than flexibility approaches;

ii) The approach is well suited to handle nonlinearities due to:

   a) kinematic and kinetics associated with the structure [14];

   b) various types of boundary and constraint conditions [14], and;

   c) material characterization [14,15].

iii) A body of established and proven algorithms which can handle various types of nonlinearities has evolved; this includes both the capability to handle static [14,15] as well as transient situations [14,16];

iv) Modelling of overall RBS systems more direct as extensive element libraries are currently available; this includes beam, plate, shell, 2-D, as well as 3-D elements [15];

v) Algorithmic adaptability.

Currently available general purpose codes such as NASTRAN, MARC, ANSYS, ARGUS, ADINA, ASKAII, NEPSAP, FESAP, SAPVI all have most of the foregoing items implemented as user features [17]. Although these codes possess the required degree of generality to model the structural aspects of jet engine rotor-stator structure, what is currently lacking are interactive "bearing type elements" and the overall algorithmic strategies to handle conservative/nonconservative interactive type forces. In turbine engine, such fields are generated in the squeeze film dampers and labyrinth seals and during rub-impact events.

In addition to the foregoing modelling difficulties, there is also a need to better quantify the effects of such factors as:

i) Rotor/stator static de-centering forces generated via:

   a) manufacturing tolerances
   b) thermal warps
   c) high "g" forces
   d) in service damage and wear,

ii) Degree of structural nonlinearity encountered,

iii) In service dynamic phenomena (rubs, impacts, etc.).

6.1 Compatibility With Proven Finite Element Codes

As noted earlier, while currently available FE codes possess the requisite generality to handle the structural aspects of RBS system modelling, no provisions are currently available to model the conservative/nonconservative effects of squeeze film damp-

ers, seals, rubs, impacts, etc. In view of this, future efforts will be given to developing a variety of special purpose "bearing elements" which can model such rotor/stator interactive force fields. These "elements" will be developed so as to be both algorithmically as well as architecturally compatible with proven FE codes. In this direction, it appears that codes such as ADINA would be the most likely software condidates about which such a development should be configured. This follows from the twofold fact that such codes have the following:

i) Extensive and well proven dynamic/element capacity,

ii) An architecture developed to allow the user to modify the overall algorithmic flow of a given solution loop.

6.2 Preliminary Engine Dynamics Analyses

The computational schemes ultimately implemented to track engine dynamic response will have to function properly over a wide spectrum of motion frequency and a wide range of nonlinearities. The development of computationally reliable interactive elements, such as the bearing/damper element, will therefore require a simplified engine dynamics analysis, using available rotor-dynamics computer codes, to realistically assess potential computational difficulties. For example, specifying the outer envelope or limits of the bearing/damper element must be predicated on a correct understanding of relative rigidities and dynamic participation of individual components in and around the bearing. These analyses include the following: (i) linear unbalance forced response, (ii) linear nonsynchronous forced

response, (iii) linear self-excited instability analysis, and (iv) simplified time-transient nonlinear analysis.

6.3 Interactive Elements for Labyrinth Seals

The typical jet engine configuration contains several labyrinth seals. The flow field within these seals results from the combined effects of rotation and pressure-gradient induced axial through flow. Depending upon the design parameters of a labyrinth seal, either a centering or decentering static radial force can be produced on the rotor. Likewise, the mechanical impedence (stiffness, damping and virtual mass) between rotor and stator at the labyrinth seal is a strong function of design details. Carefully conducted experiments by Wright [18] have recently shown that the labyrinth aerodynamic forces can be either stabilizing (positive damping) or destabilizing (negative damping) depending upon the direction of entering flow pre-swirl and the direction of rotor whirl.

The full importance of labyrinth seals to total engine dynamic analyses is therefore not confined only to the potential for rotor/stator rubs and impacts under high vibration levels. A realistic simulation of engine dynamic phenomena, linear as well as nonlinear, must therefore include a comprehensive mathematical model for the labyrinth seals which are located throughout the engine. The development and implementation of a labyrinth-seal interactive element is therefore important future work.

6.4 Rotor-Stator Rub/Impact Elements

While significant efforts have been given to developing codes which can handle the impact behavior of compressor blades, no work is currently available on modelling rotor-stator rub-impact events. Due to the structural flexibility and close tolerances inherent to gas turbine engines, such phenomena must undoubtably play an important role in defining the transient/steady state behavior during moderate and large excursion situations. Because of this, in addition to developing "bearing elements" some attention must be given to FE modelling the rotor-stator rub-impact events occurring in the labyrinth seals, and blade-case zone. Such "rub-impact elements" will have to be capable of:

i) Tracking the appropriate rotor-stator clearances

ii) Model impact-detachment mechanisms

iii) Model traction and kinematic constraints generated during rubbing

iv) Properly model energy losses occurring during such events

6.5 Rotor/Stator Static Radial Offsets Loads

The stiffness and damping characteristics of fluid film bearings are highly dependent upon their static centering or de-centering loads. Clearly, the squeeze-film dynamic forces will change considerably as static radial load is applied at the bearing since a shift of equilibrium eccentricity position will occur. Prominent sources of static radial offset loads result from each of the following:

i) Manufacturing and assembly tolerances

ii) Thermal distortions

iii) High g-force

iv) In-service damage and wear

v) Aerodynamic forces

An evaluation of these static radial offset loads is in itself a major effort. However, a realistic computer-simulation of various engine dynamic phenomena can not be accomplished without a successful effort to determine the static interactive forces between rotors and stator.

6.6 Structural Nonlinearities

In addition to modelling nonlinearities induced by the rotor/stator interactive force fields, purely structural effects may also be encountered. Such structural nonlinearities fall into two main categories:

i) Kinematic and kinetic (geometric) [14]

ii) Material characterization; plasticity, viscoplasticity

The kinematic-kinetic characterization itself falls into three main categories, namely small deflections, small strains-large rotations and moderate/large strains. Apart from highly localized events such as impact-rub zones, the most prevalent geometric modes will most probably be typified by small deflection or at most small strain-moderate rotation characterizations.

For localized rotor/stator rub-impact zones, in addition to interactive traction fields and surface machining, potential

plastic flow and moderate straining may occur. Beyond inducing outright failure, such localized fields may have a significant enough effect on the geometric configuration as to cause engine imbalance.

Because of the foregoing, the potential existence of kinematic-kinetic and constitutive nonlinearity must be accommodated in the overall model. Since the effects of such nonlinearity are fairly well localized, a partitioned linear/nonlinear approach should be employed for the finite element model.

6.7 Dynamic Loads

Emergency modes of operation, such as occur with blade failure, hard landings and foreign matter ingestion events, will require a comprehensive investigation to identify and model the resulting dynamic input loads to the engine system. Some worthwhile information could be obtained from a comprehensive engine dynamics simulation, even with postulated high amplitude dynamic input loads, such as the relative endurance of two different engine configurations. However, real-event simulation will require an accurate prior appraisal of dynamic load inputs to the engine system which result from identifiable emergency operating modes. The effort required to determine reliable estimates of dynamic input force time or frequency signature could be substantial.

As noted earlier, the engine structure must survive a rather severe operating environment. In addition to extreme thermal and aerodynamic loads, the RBS system may be subject to:

i) Transient and steady state inbalance loads

ii) Rotor-stator rub-impacts

iii) Rotor-stator decentering forces

Such events are generally caused by a combination of the following broad categories of factors:

i) Blade erosion

ii) Blade-disk-seal failure

iii) Thermal warps of rotor-stator structure due to ratcheting and creep

iv) Misalignments due to manufacturing tolerances

v) High "g" loads due to maneuvering

In view of the foregoing, future analytical modelling of RBS systems inherent to engines must employ proven computational schemes which possess the capability to handle as wide a cross-section of the loading environment as possible. As the time history of such loading events covers a wide range of time scale, the overall approach must also possess a high degree of algorithmic adaptability so as to accommodate both explicit and implicit integration schemes [16]. This is of potential importance since such schemes have been found to have varying degrees of success over various time scales [16].

6.8 Simulation of In-Service Dynamic Phenomena

The direction of future work outlined here will represent a major advancement in the state-of-the-art of engine system dynamic analysis. Proper account of structural complexities, various rotor/stator interactive forces (static and dynamic),

important nonlinearities, aerodynamic forces and well defined dynamic load inputs will provide a greatly expanded scope in the types of engine dynamics phenomena that could be studied. Engine configuration improvement studies which are impractical to accomplish through testing can then be pursued through systematic dynamic simulation studies.

Also, a better understanding of the dynamic behavior of existing engine configurations can provide valuable information leading to major reduction in engine maintenance and overhaul costs. Engine dynamic behavior is becoming progressively more important as efficiency improvement considerations push rotor/stator running clearances progressively smaller. A realistic evaluation of potential engine reliability degredation resulting from smaller rotor/stator running clearances demands the high level of dynamic system simulation described here.

Section 7

CONCLUSIONS

General engine dynamic analyses which properly account for rotor-to-stator and rotor-to-rotor interactive forces can be approached through the use of available general purpose nonlinear finite-element computer codes. Interactive forces originating at bearing squeeze-film dampers and rub-impact events are, however, not available with general purpose codes at this time. The work described herein shows the viability of using general purpose finite-element codes for engine dynamic analysis. Also, the four-degree-of-freedom example model demonstrates the use of the

squeeze-film damper code developed in this work. Results with this demonstration model are consistent with the results of other investigators of nonlinear squeeze-film damper dynamics.

REFERENCES

1. Fertis, D. G., "Dynamics and Vibrations of Structures", John Wiley and Sons Company, Inc., New York, NY, 1973.

2. Hibner, D. H., "Dynamic Response of Viscous-Damped Multi-Shaft Jet Engines," AIAA Journal of Aircraft, Vol. 12, 1975, pp 305-312.

3. Adams, M. L., "Nonlinear Dynamics of Multi-Bearing Flexible Rotors," Journal of Sound and Vibration, Vol. 71 (1), 1980, pp 129-144.

4. Green, A. E. and Adkins, J. E., "Large Elastic Deformations," Oxford Press, England, 1960.

5. Chang, T. Y. and Padovan, J., "General Purpose Finite Element Programs," presented at ASME Pressure Vessel Conference, San Francisco, CA, June 1979.

6. Padovan, J. and Chang, T. Y., "Evaluation of ADINA Part II Operating Characteristics," ONR Contract N-00014-78-C-0691.

7. Bathe, K. J., "ADINA - A Finite Element Program for Automatic Dynamic Incremental Nonlinear Analysis," Report 82448-1, Acoustic Lab., Mechanical Engineering Dept., MIT, May 1976 (revised 1977).

8. Padovan, J., "Self-Adaptive Incremental Newton-Raphson Algorithms," Symposium on Computational Methods in Nonlinear Structural and Solid Mechanics," Washington, October, 1980.

9. Newmark, N. M., "A Method of Computation for Structural Dynamics," Journal of Engineering Mechanics Division ASCE, Vol. 8, pp 67, 1959.

10. Wilson, E. L., "A Computer Program for the Dynamic Stress Analysis of Underground Structures," SESM Report No. 68-1. University of California, Berkeley, 1968.

11. Houbolt, "A Recurrence Matrix Solution for the Dynamic Response of Elastic Aircraft," Journal of Aeronautical Society, Vol. 17, pp. 540, 1950.

12. Hughes, T. J. R., "Stability, Convergence and Growth and Decay of Energy of the Average Acceleration Method in Nonlinear Structural Dynamics," Journal Comp. and Struct., Vol. 6, pp 313, 1976.

13. Felippa, C. A. and Park, K. C., "Direct Time Integration Methods in Nonlinear Structural Dynamics," Comp. Meth. Appl. Mech. Eng., pp 277, 1979.

14. Belytschko, T., "Nonlinear Analyses-Descriptions and Numerical Stability," Computer Programs in Shock and Vibration, Ed., W. Pilkey and B. Pilkey, Shock and Vibration Information Center, Washington, D.C., pp 537 (1975).

15. Zienkiewicz, O. C., "The Finite Element Method," McGraw Hill, London (1977).

16. Felippa, C.A. and Park, K.C., "Direct Time Integration Methods in Nonlinear Structural Dynamics," presented at FENOMECH, University of Stuttgart (1978).

17. Structural Mechanics Computer Programs, edited by Pilkey, W., Saczalski, K. and Schaeffer, H., University Press of Virginia, Charlottsville (1975).

18. Wright, D. V., "Air Model Tests of Labyrinth Seal Forces on a Whirling Rotor," Trans, ASME Journal of Engineering for Power, 1978, Vol. 100, pp 533-543.

19. O'Donoghue, J. P., Koch, P. R. and Hooke, C. J., "Approximate Short Bearing Analysis and Experimental Results Obtailed Using Plastic Bearing Liners," Proc. Institute of Mechanical Engineers, Vol. 184, 1969, pp 190-196.

20. Rhode, S. M. and Li, D. F., "A Generalized Short Bearing Theory," Trans. ASME Journal of Lubrication Technology, Vol. 102, No. 3, 1980, pp 278-282.

21. Barrett, L. E., Allaire, P. E. and Gunter, E. J., "A Finite Length Bearing Correction Factor for Short Bearing Theory," Trans. ASME Journal of Lubrication Technology, Vol. 102, No. 3, 1980, pp 283-290.

APPENDIX A

Damper Element Fortran Listing

```
LIST UTILITY

      SUBROUTINE SQUEEZ(AD,AL,AC,AISC,ATH1,ATH2,AB1,AB2,U,V,
C
     1 UDT,VDT,UB,VB,UBT,VBT,AK11,AK12,AK22,AC11,AC22,F1,F2,NGRIA,NSOLA,
C
     2 NPORA,KAFK,KAFC,NFILA,PVAA)
C     NONLINEAR TIME-TRANSIENT SQUEEZE-FILM DAMPER INTERACTIVE ELEMENT
C     THIS CODE COMPUTES INSTANTANEOUS FORCE VECTOR AND ITS
C     SPATIAL GRADIENTS, I.E., THE TANGENT STIFFNESS AND DAMPING
C     MATRICES.
C
C     ------------
C     NOMENCLATURE
C     ------------
C     INPUT
C     -----
C     BD=NOMINAL DAMPER ANNULUS DIAMETER(IN)
C     BL=NOMINAL DAMPER ANNULUS LENGTH(IN)
C     BC=DAMPER ANNULUS RADIAL CLEARANCE(IN)
C     VISC=DAMPER LUBRICANT VISCOSITY(REYNS)
C     PVAP=FILM RUPTURE PRESSURE(PSIA)
C     THT(1)=POSITION ANGLE OF LUBRICANT PORT-1(DEG)
C     THT(2)=POSITION ANGLE OF LUBRICANT PORT-2(DEG)
C     PB(1)=SPECIFIED BOUNDARY PRESSURE AT PORT-1(PSIA)
C     PB(2)=SPECIFIED BOUNDARY PRESSURE AT PORT-2(PSIA)
C     NGRID=NUMBER OF FINITE-DIFFERENCE GRID POINTS PER DAMPER ARC(ODD)
C     NSOLN=1,LONG-BEARING SOLUTION USED
C           =2,SHORT-BEARING(PARABOLIC) SOLUTION USED
C           =3,FOURIER-SERIES 2-D CONVERGENT SOLUTION USED
C     NPORT=NUMBER OF LUBRICANT PORTS(0,1 OR 2)
C           IF NPORT=0, JOINED-BOUNDARY CONDITION IS USED
C     NFILM=NUMBER OF IDENTICAL ANNULI FOR THE DAMPER
C     KOFK=0,STIFFNESS MATRIX NOT COMPUTED
```

```
LIST UTILITY
C
C     KOFK=1,STIFFNESS MATRIX COMPUTED
C
C     KOFC=0,DAMPING MATRIX NOT COMPUTED
C
C     KOFC=1,DAMPING MATRIX COMPUTED
C
C     X=X-INERTIAL COORDINATE OF DAMPER INSIDE SURFACE CENTER-LINE(IN)
C
C     Y=Y-INERTIAL COORDINATE OF DAMPER INSIDE SURFACE CENTER-LINE(IN)
C
C     XDT=X-INERTIAL VELOCITY OF INSIDE SURFACE CENTER-LINE(IN/SEC)
C
C     YDT=Y-INERTIAL VELOCITY OF INSIDE SURFACE CENTER-LINE(IN/SEC)
C
C     XB=X-INERTIAL COORDINATE OF DAMPER OUTSIDE SURFACE CENTER-LINE(IN)
C
C     YB=Y-INERTIAL COORDINATE OF DAMPER OUTSIDE SURFACE CENTER-LINE(IN)
C
C     XBT=X-INERTIAL VELOCITY OF DAMPER OUTSIDE SURFACE CENTER-LINE(IN)
C
C     YBT=Y-INERTIAL VELOCITY OF DAMPER OUTSIDE SURFACE CENTER-LINE(IN)
C
C
C     OUTPUT
C     ======
C
C     F1=X-FORCE COMPONENT ON INSIDE DAMPER SURFACE(LBS)
C
C     F2=Y-FORCE COMPONENT ON INSIDE DAMPER SURFACE(LBS)
C
C     FORCE COMPONENTS ON OUTSIDE DAMPER SURFACE ARE EQUAL BUT OPPOSITE
C
C     F1 AND F2 BECAUSE FLUID INERTIA EFFECTS ARE NEGLECTED
C
C     SYMMETRIC PORTION OF STIFFNESS MATRIX:
C
C          AK11=KXX(LBS/IN)
C
C          AK12=KXY(LBS/IN)=KYX
C
C          AK22=KYY(LBS/IN)
C
C     DIAGONAL PORTION OF DAMPING MATRIX
C
C          AC11=CXX(LB*SEC/IN)
C
C          AC22=CYY(LB*SEC/IN)
C
      IMPLICIT REAL*8 (A-H,O-Z)
C
      COMMON/INPUT1/BD,BL,BC,VISC,THT(2),PB(2),PVAP
C
      COMMON/INPUT2/NGRID,NSOLN,NPCRT,NFILM
C
      COMMON/COORD/X,Y,XDT,YDT,XB,YB,XBT,YBT
C
      COMMON/FILM/TH(101),H(101),DHDX(101),DHDT(101),STH(101),CTH(101),
```

```
LIST UTILITY

C
      1DXD(2),ALFA(2)
C
       COMMON/WORK/FNGDM1,KB,KOUNT
C
       COMMON/INC/HMIN,VEL,DELS,DELST
C
       DIMENSION A(101),B(101),C(101),E(101),RH(101),P(101),ARG1(101),
C
      1 ARG2(101),D(101)
C
C      ALLOCATE INPUT NAMES
C
       BD     = AD
       BL     = AL
       BC     = AC
       VISC   = AISC
       THT(1)= ATH1
       THT(2)= ATH2
       PB(1) = AB1
       PB(2) = AB2
       PVAP   = PVAA
       X      = U
       Y      = V
       XDT    = UDT
       YDT    = VDT
       XB     = UB
       YE     = VB
       XBT    = UBT
       YBT    = VBT
       NGRID = NGRIA
       NSOLN = NSOLA
       NPORT = NPORA
       KOFK   = KAFK
       KOFC   = KAFC
       NFILM = NFILA
       PI     = 3.141592654
C      WRITE (6,2500) X,Y,XE,YB,XDT,YDT,XBT,YBT
 2500 FORMAT (7X,'X-ROTOR',5X,'Y-ROTOR',5X,'X-STATOR',4X,'Y-STATOR',
     3          5X,'ROTOR XDT',
     1          5X,'ROTOR YDT',4X,'STATOR XDT',5X,'STATOR YDT',//,
     2          5X,8(2X,D13.6))
C
C      WRITE (6,1999)
 1999 FORMAT (///////,4X,'BEARING ELEMENT INFORMATION',//,4X,
C
     1          ' BD           BL           BC           VISC   '
C
     2         ,'PVAP         TH1          TH2          PB1          PB2          NG
C
     3  NS    NP    NF   KK   KC')
C      WRITE(6,10)BD,BL,BC,VISC,PVAP,THT(1),THT(2),PB(1),PB(2),
C     1           NGRID,NSOLN,NPORT,NFILM,KOFK,KOFC
   10 FORMAT (9D11.4,4I5,2I4)
C
C      SET UP
C
       KOUNT    = 1
```

```
LIST UTILITY

      MTEST    = NGRID + 1
      NTEST    = MTEST/2
      KTEST    = 2*NTEST
C
      IF(KTEST.NE.MTEST) NGRID=NGRID-1
C
      FNGDM1   = FLOAT(NGRID-1)
      THT(1)   = THT(1)*PI/180.
C
      IF(NPORT.LT.2) GO TO 20
C
      THT(2)   = THT(2)*PI/180.
C
      IF(THT(2).LT.THT(1)) THT(2)=THT(2)+2.*PI
C
      ALFA(1) = THT(2)-THT(1)
      ALFA(2) = 2.*PI-ALFA(1)
      DXD(1)   = 0.5*BD*ALFA(1)/FNGDM1
      DXD(2)   = 0.5*BD*ALFA(2)/FNGDM1
C
      GO TO 40
C
   20 DXD(1)   = BD*PI/FNGDM1
      ALFA(1) = 2.*PI
C
   40 CONTINUE
C
C     WRITE(6,10)DXD(1),DXD(2)
      AKXX = 0.0
      AKXY = 0.0
      AKYX = 0.0
      AKYY = 0.0
      ACXX = 0.0
      ACXY = 0.0
      ACYX = 0.0
      ACYY = 0.0
      FX   = 0.0
      FY   = 0.0
C
C     BRANCH ACCORDING TO SOLUTION DESIGNATED
C
   60 CONTINUE
      CALL INCRNT
      GO TO (100,100,300),NSOLN
  100 CONTINUE
C
C     SOLVE FOR SQUEEZE FILM PRESSURE DISTRIBUTION
C
      DO 190 KB=1,NPORT
      P(1)=PB(KB)
      IF(KB.EQ.1) P(NGRID)=PB(2)
      IF(KB.EQ.2) P(NGRID)=PB(1)
      DX=DXD(KB)
      CALL DFILM
      A(2)=0.0
      B(2)   = P(1)
      DO 110 K=2,NGRID
      COEF1 = H(K)**3/DX**2
```

LIST UTILITY

```
      COEF2 = (1.5*H(K)**2)*DHDX(K)/DX
      C(K)  =-2.*COEF1
      D(K)  = COEF1+COEF2
      E(K)  = COEF1-COEF2
      RH(K) = 12.*VISC*DHDT(K)
      IF(NSOLN.EQ.1) GO TO 110
      C(K)  = C(K)-(8.*H(K)**3)/BL**2
  110 CONTINUE
      NGRD  = NGRID-1
      DO 120 K=2,NGRD
      FOCTR = C(K)+E(K)*A(K)
      A(K+1)=-D(K)/FOCTR
  120 B(K+1)=(RH(K)-E(K)*B(K))/FOCTR
      NGR   = NGRID-2
      DO 130 K=1,NGR
      J     = NGRID-K
      P(J)  = A(J+1)*P(J+1)+B(J+1)
      IF(P(J).LT.PVAP) P(J)=PVAP
  130 CONTINUE
C     WRITE(6,135)(P(J),J=1,NGRID)
  135 FORMAT(2X,14E9.2)
C
C     INTEGRATE PRESSURE DISTRIBUTION TO GET X AND Y FORCE COMPONENTS
C
      DO 140 K=1,NGRID
      ARG1(K)  = P(K)*CTH(K)
  140 ARG2(K)  = P(K)*STH(K)
      A1       = ARG1(1)+ARG1(NGRID)
      A2       = ARG2(1)+ARG2(NGRID)
      B1       = 0.0
      B2       = 0.0
      DO 150 K=2,NGRD,2
      B2 = B2+ARG2(K)
  150 B1 = B1+ARG1(K)
      C1 = 0.0
      C2 = 0.0
      DO 160 K=3,NGR,2
      C1=C1+ARG1(K)
  160 C2=C2+ARG2(K)
      DTHET=2.*DX/BD
      FACTR=FLOAT(NFILM)*DTHET/3.
      XQ=FACTR*(A1+4.*B1+2.*C1)
      YQ=FACTR*(A2+4.*B2+2.*C2)
      IF(NSOLN.EQ.1) FACTR=-BD*BL/2.
      IF(NSOLN.EQ.2) FACTR=-BD*BL/3.
      XQ=XQ*FACTR
      YQ=YQ*FACTR
      FX=FX+XQ
      FY=FY+YQ
  190 CONTINUE
      GO TO (500,520,540,560,580),KOUNT
  500 F1=FX
      F2=FY
      IF((KOFK.EQ.0).AND.(KOFC.EQ.0)) RETURN
      IF(KOFK.EQ.0) KOUNT=4
      IF(KOFK.EQ.0) GO TO 60
      GO TO 590
  520 AKXY=(FX-F1)/DELS
```

LIST UTILITY

```
      AKYX=(FY-F2)/DELS
      GO TO 590
  540 AKXY=(FX-F1)/DELS
      AKYY=(FY-F2)/DELS
C     WRITE (6,657) AKXX,AKXY,AKYY
  657 FORMAT (5X,'BEARING STIFF.(SQUEEZ):  ',3(5X,D13.6))
      AK11=-AKXX
      AK22=-AKYY
      AK12=-0.5*(AKXY+AKYX)
C     WRITE (6,657) AK11,AK12,AK22
C     WRITE (6,658) F1,F2
  658 FORMAT (5X,'FORCES ON THE ROTOR:',//,8(2X,D13.5))
      IF(KOFC.EQ.0) RETURN
      GO TO 590
  560 ACXX=(FX-F1)/DELST
      ACYX=(FY-F2)/DELST
      GO TO 590
  580 ACXY=(FX-F1)/DELST
      ACYY=(FY-F2)/DELST
      GO TO 600
  590 KOUNT=KOUNT+1
      GO TO 60
  600 CONTINUE
      AC11=-ACXX
      AC22=-ACYY
      RETURN
  300 WRITE(6,700)
      RETURN
  700 FORMAT(1H1//5X'FOURIER-SERIES 2-D OPTION NOT READY FOR USE'//)
      END
//??
//
//??
```

322 RECORDS PRINTED. END OF LIST UTILITY

APPENDIX B

Simple System "Driver" Fortran Listing

LIST UTILITY

```
//NASA      JOB  04180,'7663ADAMS'          ',MSGLEVEL=(2,0)
/*JOBPARM TIME=9
// EXEC FORT
C
C      FOUR DOF ROTOR/BEARING/STATOR SYSTEM
C
      DIMENSION XS(1002),YS(1002),XBS(1002),YBS(1002),XREL(1002),
     1YREL(1002),NPTS(2),INC(2)
      DIMENSION XT(2002),YT(2002)
      DIMENSION LINTYP(2),INTEQ(2)
      CALL PLOTS
      CALL PLOT(1.0,1.5,-3)
      IN=5
      IO=6
    5 CONTINUE
      KUNT=0
      READ(IN,10)BD,BL,BC,VISC,TH1,TH2,PB1,PB2,E,CPM1,PHI1,PVAP
   10 FORMAT(5E15.7)
      READ(IN,15)NGRID,NSOLN,NPORT,NCYC,NDTPC,KOFK,KOFC,NFILM
   15 FORMAT(16I5)
      PI=3.141592654
      WRITE(IO,20)
   20 FORMAT(1H1///)
      WRITE(IO,25)BD,BL,BC,VISC,TH1,TH2,PB1,PB2,E,CPM1,PHI1,PVAP
   25 FORMAT(2X12E10.3///)
      WRITE(IO,30)NGRID,NSOLN,NPORT,NCYC,NDTPC,KOFK,KOFC,NFILM
   30 FORMAT(2X10I10)
      READ(IN,10)RMASS,SMASS,RFORCE,SKX,SKY
      READ(IN,10)X,Y,XDT,YDT,XB,YB,XBT,YBT,WX,WY
      READ(IN,15)NPRINT,KPLOT,LINTP,NSKIP,KLUE
      RMASS=RMASS/386.
      SMASS=SMASS/386.
      PHI1=PHI1*PI/180.
      TAU1=60./CPM1
      DT=TAU1/FLOAT(NDTPC)
      NTS=NCYC*NDTPC+1
      OM1=PI*CPM1/30.
      WRITE(IO,35)
   35 FORMAT(1H1//5X'NT',8X,'TIME',11X,'X',11X,'Y',10X,'XB',10X,'YB',
     1 10X,'RX',10X,'RY',10X,'SX',10X,'SY'//)
      DO 50 NT=1,NTS
      NTM1=NT-1
      T=DT*FLOAT(NT-1)
      IF(NT.GE.NPRINT)WRITE(IO,45)NTM1,T,X,Y,XB,YB,XDT,YDT,XBT,YBT
      IF(KPLOT.EQ.0) GO TO 43
      MAA=(NT-1)/NSKIP
      MAB=NSKIP*MAA
      MAC=NT-1
      IF((NT.EQ.1).OR.(MAB.EQ.MAC)) GO TO 40
      GO TO 43
   40 KUNT=KUNT+1
      XS(KUNT)=X
      YS(KUNT)=Y
      XBS(KUNT)=XB
      YBS(KUNT)=YB
   43 CONTINUE
   45 FORMAT(2X,I5,9E12.3)
```

```
LIST UTILITY

      OM1T=OM1*T
      ARG=OM1T+PHI1
      SARG=SIN(ARG)
      CARG=COS(ARG)
      CALL SQUEEZ(BD,BL,BC,VISC,TH1,TH2,PB1,PB2,X,Y,XDT,YDT,XB,YB,
     1 XBT,YBT,AK11,AK12,AK22,AC11,AC22,F1,F2,NGRID,NSOLN,NPORT,KOFK,
     2 KOFC,NFILM,PVAP)
      RFX=RFORCE*CARG+F1+WX
      RFY=RFORCE*SARG+F2+WY
      SFX=-F1-SKX*XB
      SFY=-F2-SKY*YB
      RXA=RFX/RMASS
      RYA=RFY/RMASS
      SXA=SFX/SMASS
      SYA=SFY/SMASS
      XDT=XDT+RXA*DT
      YDT=YDT+RYA*DT
      XBT=XBT+SXA*DT
      YBT=YBT+SYA*DT
      X=X+XDT*DT
      Y=Y+YDT*DT
      XB=XB+XBT*DT
      YB=YB+YBT*DT
   50 CONTINUE
      IF(KFLOT.EQ.0) GO TO 100
      INTEQ(1)=89
      INTEQ(2)=98
      LINTYP(1)=LINTP
      LINTYP(2)=LINTP
      NPTS(1)=KUNT
      NPTS(2)=KUNT
      INC(1)=1
      INC(2)=1
      DO 80 K=1,KUNT
      XT(K)=XS(K)
      YT(K)=YS(K)
      XT(KUNT+K)=XBS(K)
      YT(KUNT+K)=YBS(K)
      XREL(K)= XS(K)-XBS(K)
   80 YREL(K)= YS(K)-YBS(K)
      CALL PLOT(12.0,0.0,-3)
      CALL GRAPH1(XS,YS,XBS,YBS,XT,YT,NPTS,INC,LINTYP,INTEQ,KUNT)
      CALL PLOT(12.0,0.0,-3)
      NPST=KUNT
      INK=1
      INTQ=89
      CALL GRAPH2          (XREL,YREL,NPST,INK,LINTP,INTQ,KUNT,BC)
  100 CONTINUE
      IF(KLUE.EQ.0) GO TO 150
      GO TO 5
  150 CALL PLOT(10.0,0.0,999)
      STOP
      END
      SUBROUTINE GRAPH1(XS,YS,XBS,YBS,XT,YT,NPTS,INC,LINTYP,INTEQ,KUNT)
      DIMENSION XS(1002),YS(1002),XBS(1002),YBS(1002),XREL(1002),
     1YREL(1002),NPTS(2),INC(2)
      DIMENSION LINTYP(2),INTEQ(2)
      DIMENSION XT(2002),YT(2002)
```

```
LIST UTILITY

      K2UNT=2*KUNT
      K2UNT1=K2UNT+1
      K2UNT2=K2UNT+2
      KUNT2=KUNT+2
      KUNT1=KUNT+1
      CALL SCALE (XT,7.5,K2UNT,INC(1))
      CALL SCALE (YT,7.5,K2UNT,INC(1))
      XS(KUNT1)=XT(K2UNT1)
      YS(KUNT1)=YT(K2UNT1)
      XS(KUNT2)=XT(K2UNT2)
      YS(KUNT2)=YT(K2UNT2)
      IF(XS(KUNT2).GE.YS(KUNT2)) GO TO 10
      XBS(KUNT2)=YS(KUNT2)
      YBS(KUNT2)=YS(KUNT2)
      XS(KUNT2)=YS(KUNT2)
      GO TO 20
   10 YS(KUNT2)=XS(KUNT2)
      XBS(KUNT2)=XS(KUNT2)
      YBS(KUNT2)=XS(KUNT2)
   20 XBS(KUNT1)=XS(KUNT1)
      YBS(KUNT1)=YS(KUNT1)
   40 CONTINUE
      CALL AXIS (0.0,0.0,'X-DISPL',-6,7.5,0.0,XS(KUNT1),XS(KUNT2))
      CALL AXIS (0.0,0.0,'Y-DISPL',6,7.5,90.0,YS(KUNT1),YS(KUNT2))
      CALL LINE(XS,YS,NPTS(1),INC(1),LINTYP(1),INTEQ(1))
      CALL LINE (XBS,YBS,NPTS(2),INC(2),LINTYP(2),INTEQ(2))
      CALL SYMBOL (0.5,7.75,0.14,'ROTOR AND STATOR ORBITS',0.0,23)
      RETURN
      END
      SUBROUTINE GRAPH2 (XREL,YREL,NPST,INK,LINTP,INTQ,KUNT,BC)
      DIMENSION XREL(1002),YREL(1002),XC(402),YC(402)
      KUNT1=KUNT+1
      KUNT2=KUNT+2
      DO 762 K=1,400
      Z=K/60.
      XC(K)=BC*COS(Z)
      YC(K)=BC*SIN(Z)
  762 CONTINUE
      CALL SCALE (XC,7.5,400,1)
      YC(401)=XC(401)
      YC(402)=XC(402)
      CALL AXIS(0.0,0.0,'REL X-DISPL',-11,7.5,0.0,XC(401),XC(402))
      CALL AXIS(0.0,0.0,'REL Y-DISPL',11,7.5,90.0,YC(401),YC(402))
      CALL LINE(XC,YC,400,1,0,0)
      XREL(KUNT1)=XC(401)
      YREL(KUNT1)=XC(401)
      XREL(KUNT2)=XC(402)
      YREL(KUNT2)=XC(402)
      CALL LINE(XREL,YREL,NPST,INK,LINTP,INTQ)
      CALL SYMBOL (0.5,7.75,0.14,'ROTOR ORBIT RELATIVE TO STATOR',0.0,
     $30)
      RETURN
      END
```

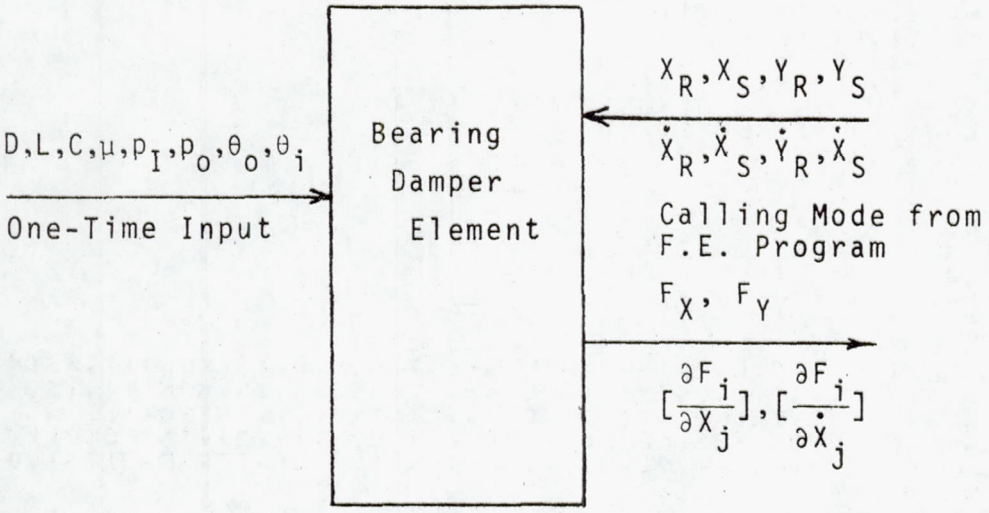

Fig.1 Input/Output of Damper Pilot Code

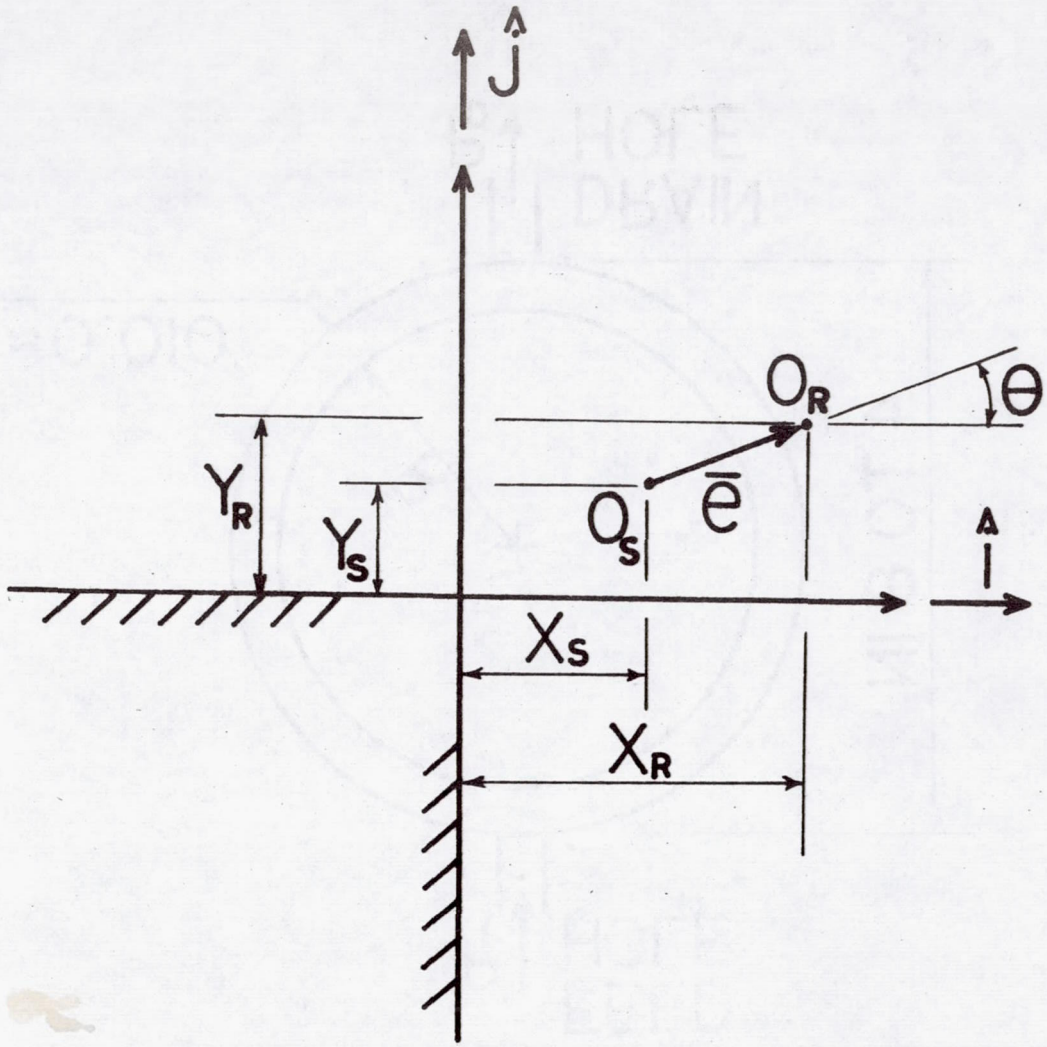

Fig. 2 Inertial coordinates

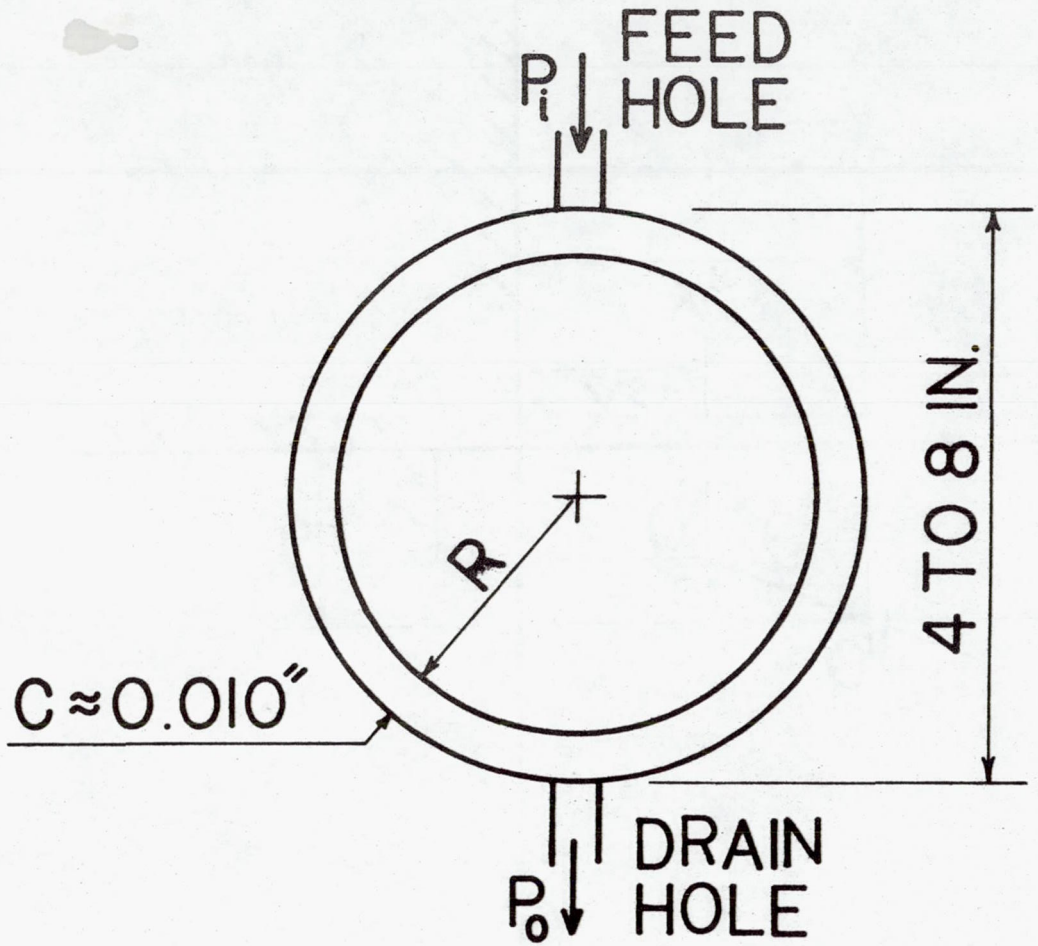

Fig. 3 A typical aircraft engine damper configuration

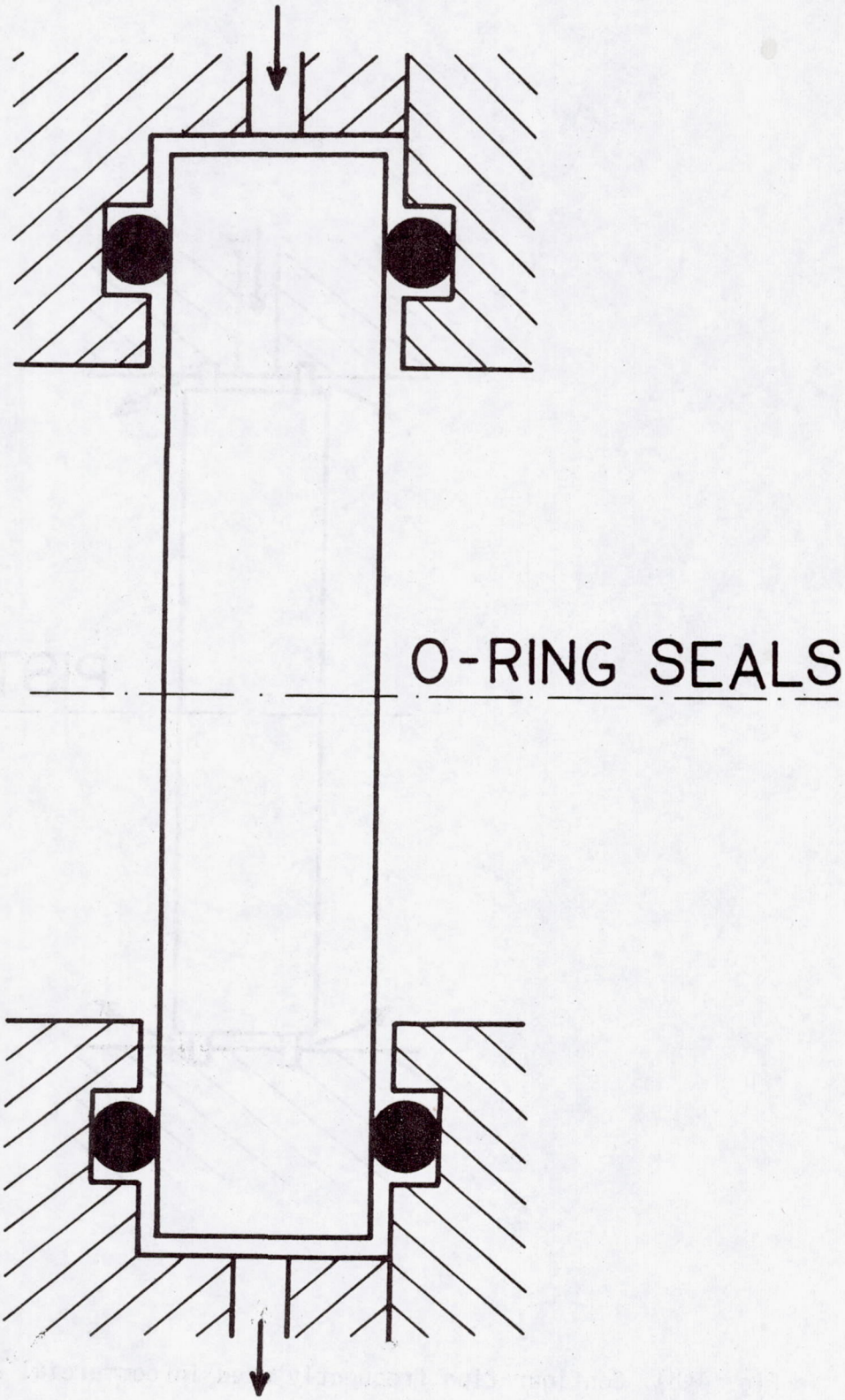

Fig. 4(a) Configuration frequently used in military applications

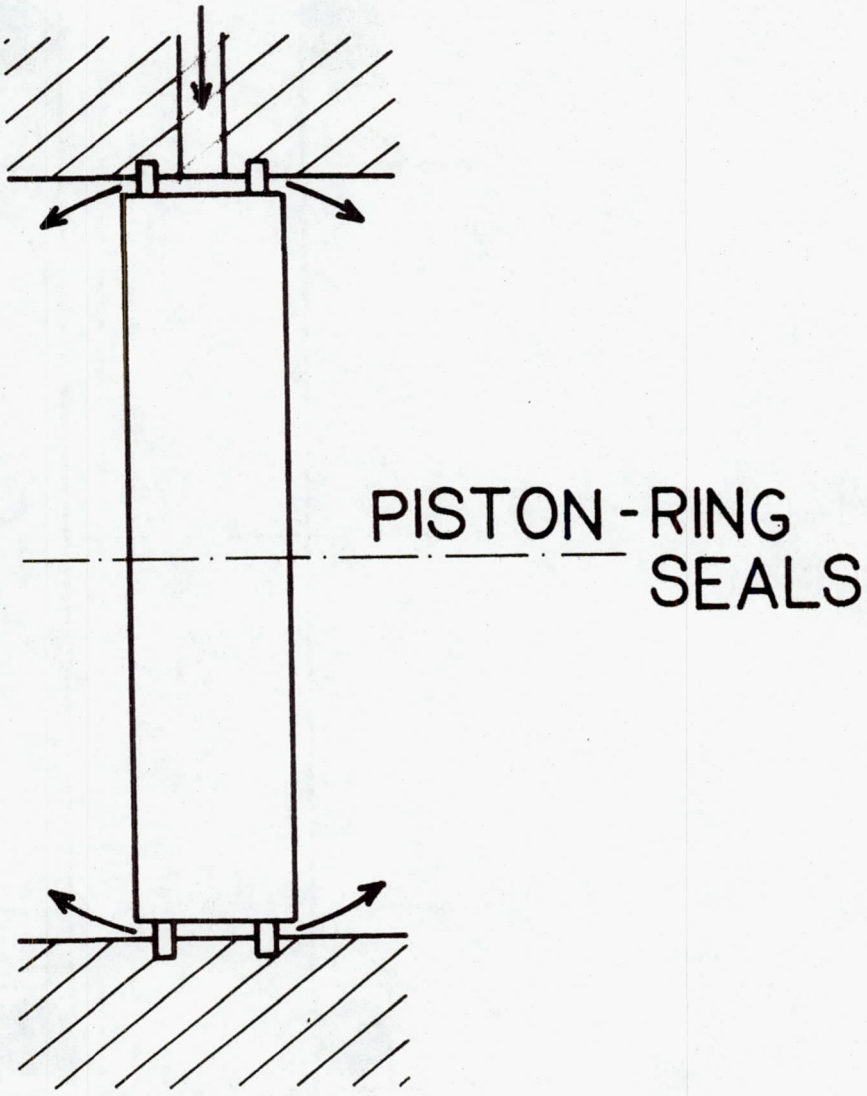

Fig. 4(b) Configuration frequently used in commercial applications

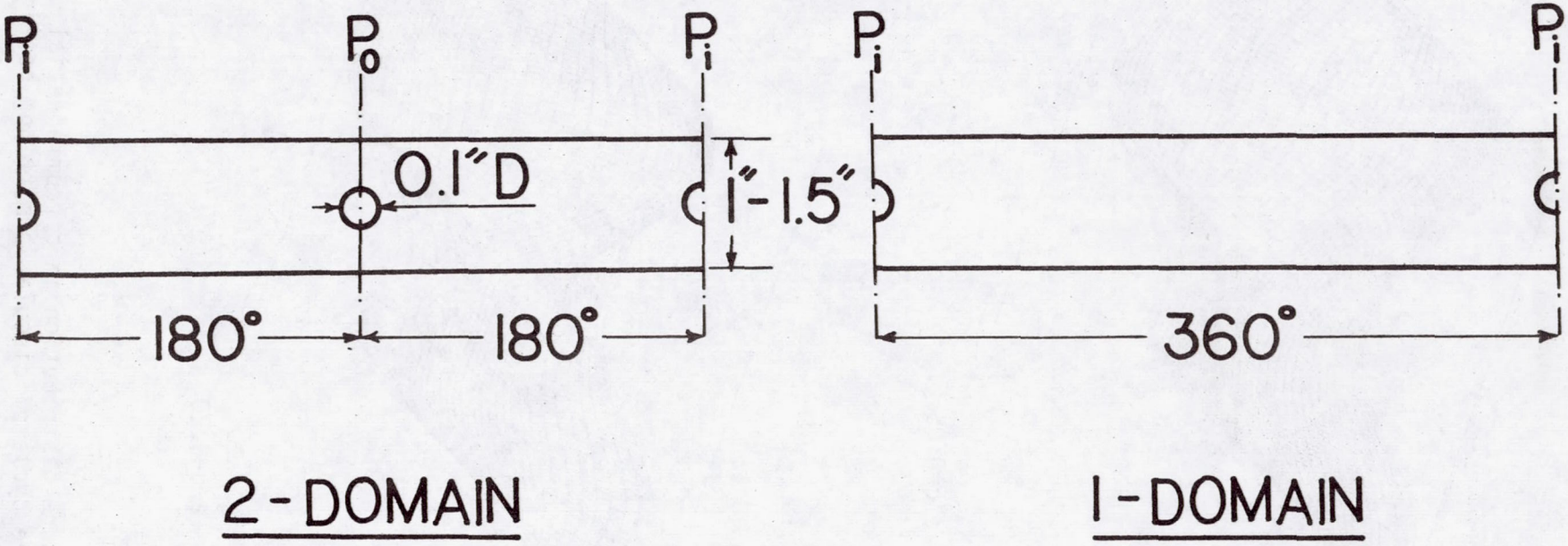

Fig. 5 Unwrapped squeeze-film pressure solution domains for configurations shown in Figure 4.

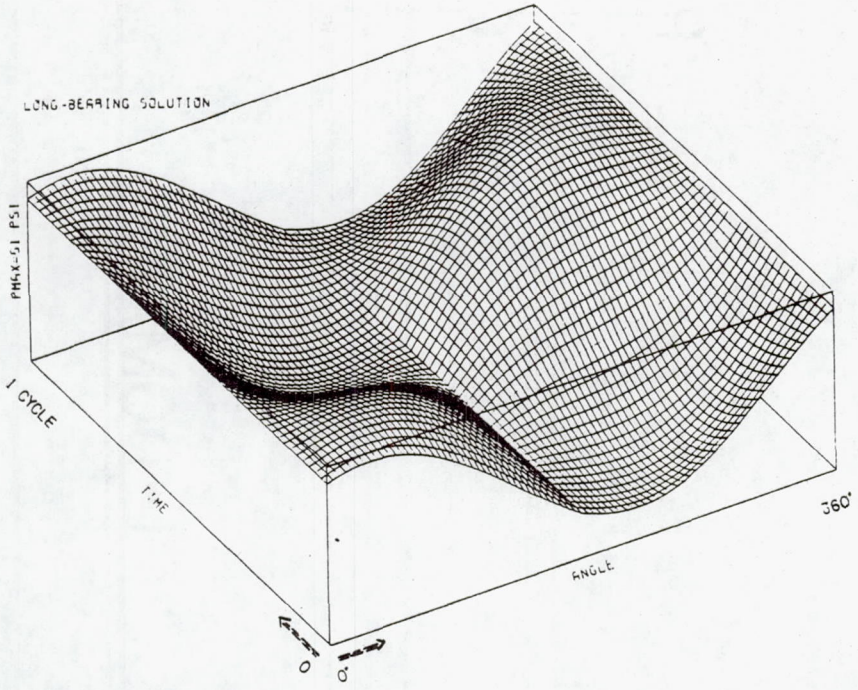

(a) e/c=0.05

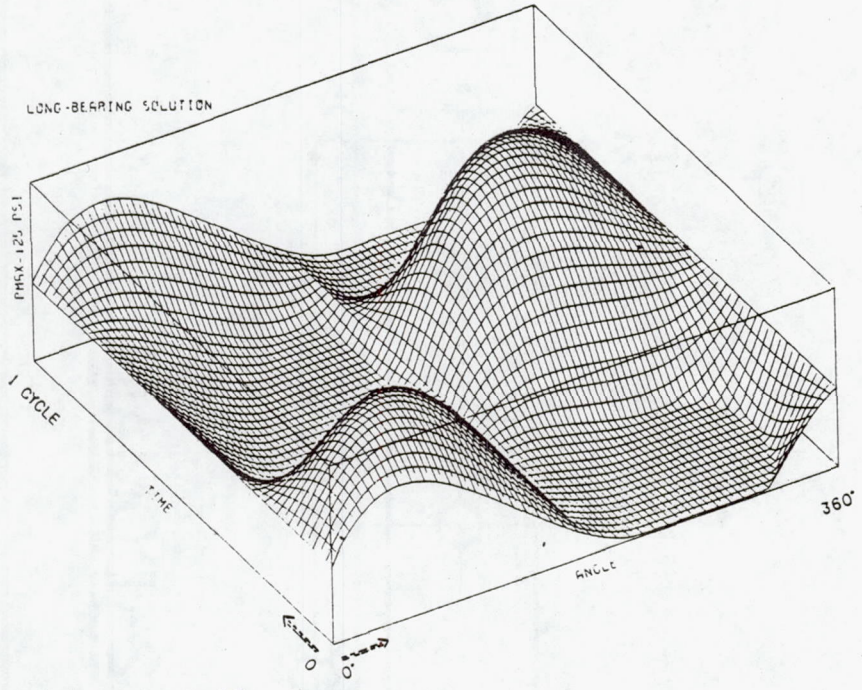

(b) e/c=0.20

Figure 6 Pressure distribution in circumferential direction and time of one cycle of circular orbit(long-bearing solution).

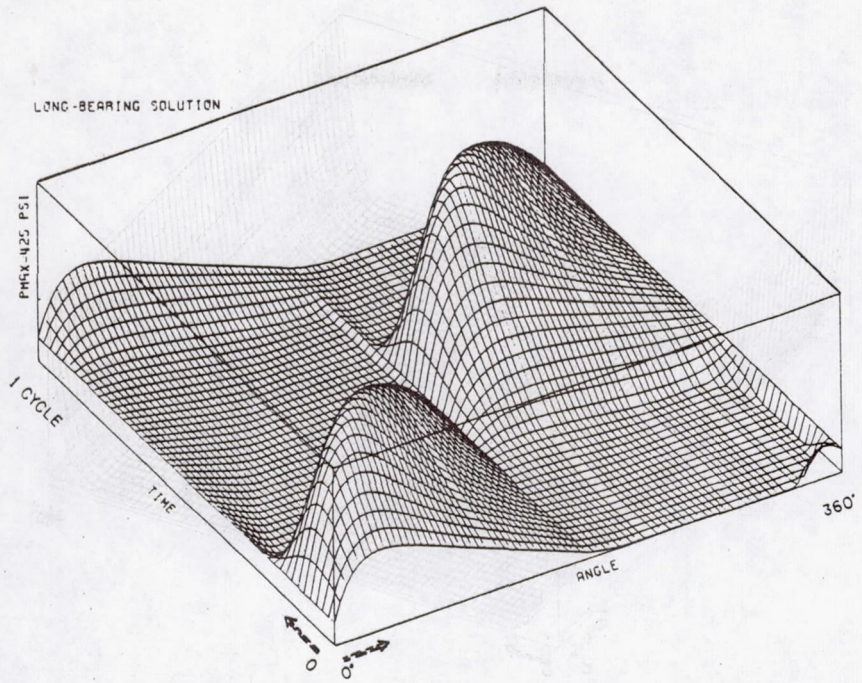

(c) e/c=0.60

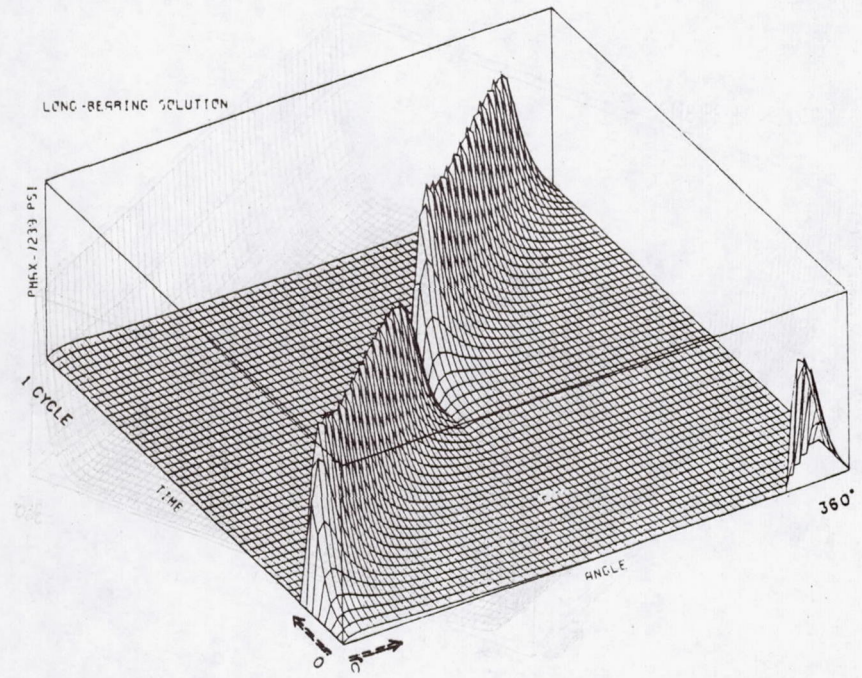

(d) e/c=0.95

Figure 6 (Cont'd) Pressure distribution in circumferential direction and time of one cycle of circular orbit (long-bearing solution).

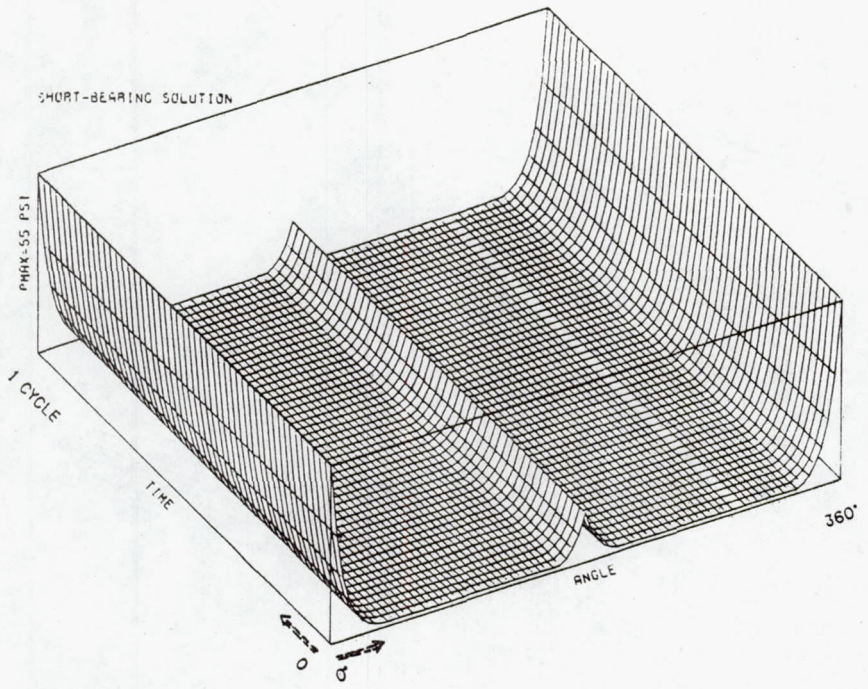

(a) e/c=0.05

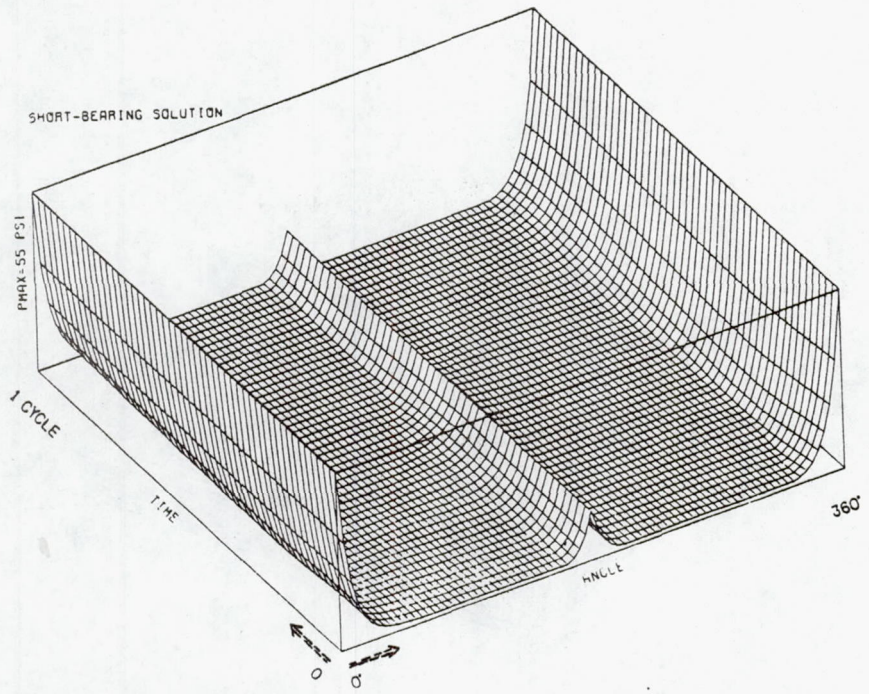

(b) e/c=0.20

Figure 7 Pressure distribution in circumferential direction and time of one cycle of circular orbit (short-bearing solution).

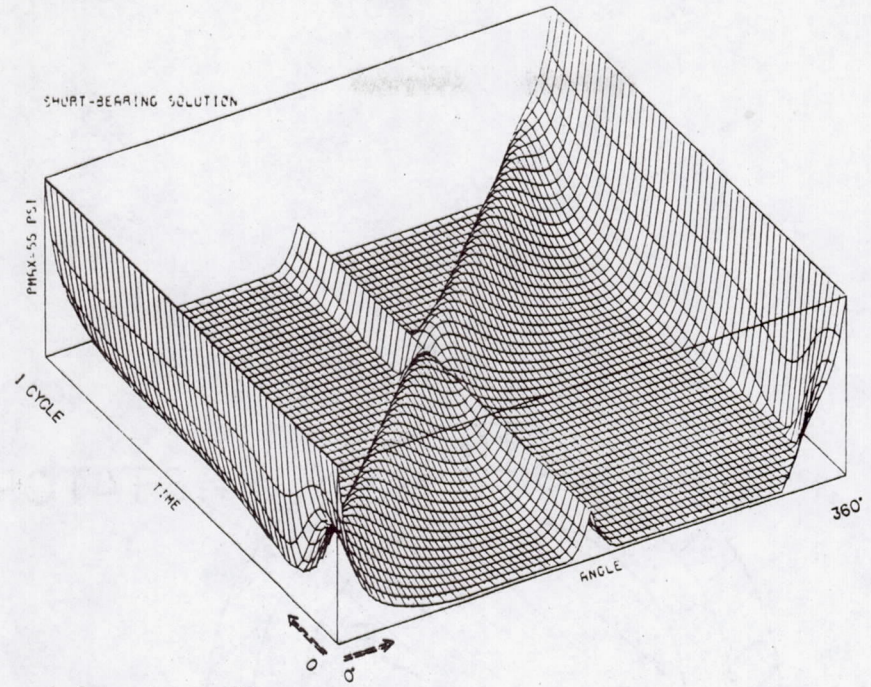

(c) e/c=0.60

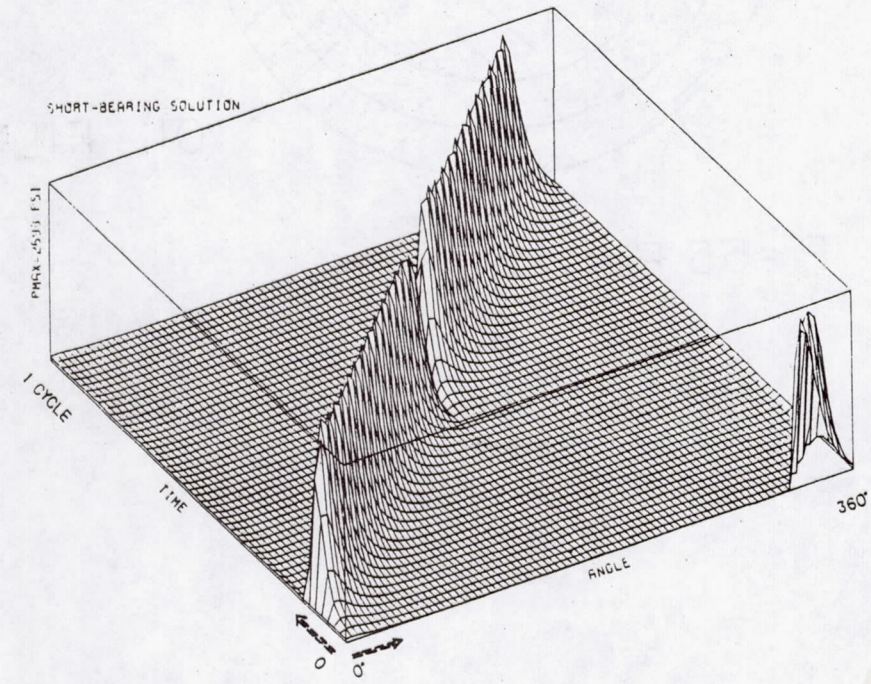

(d) e/c=0.95

Figure 7 Pressure distribution in circumferential direction and time (Cont'd) of one cycle of circular orbit (short-bearing solution).

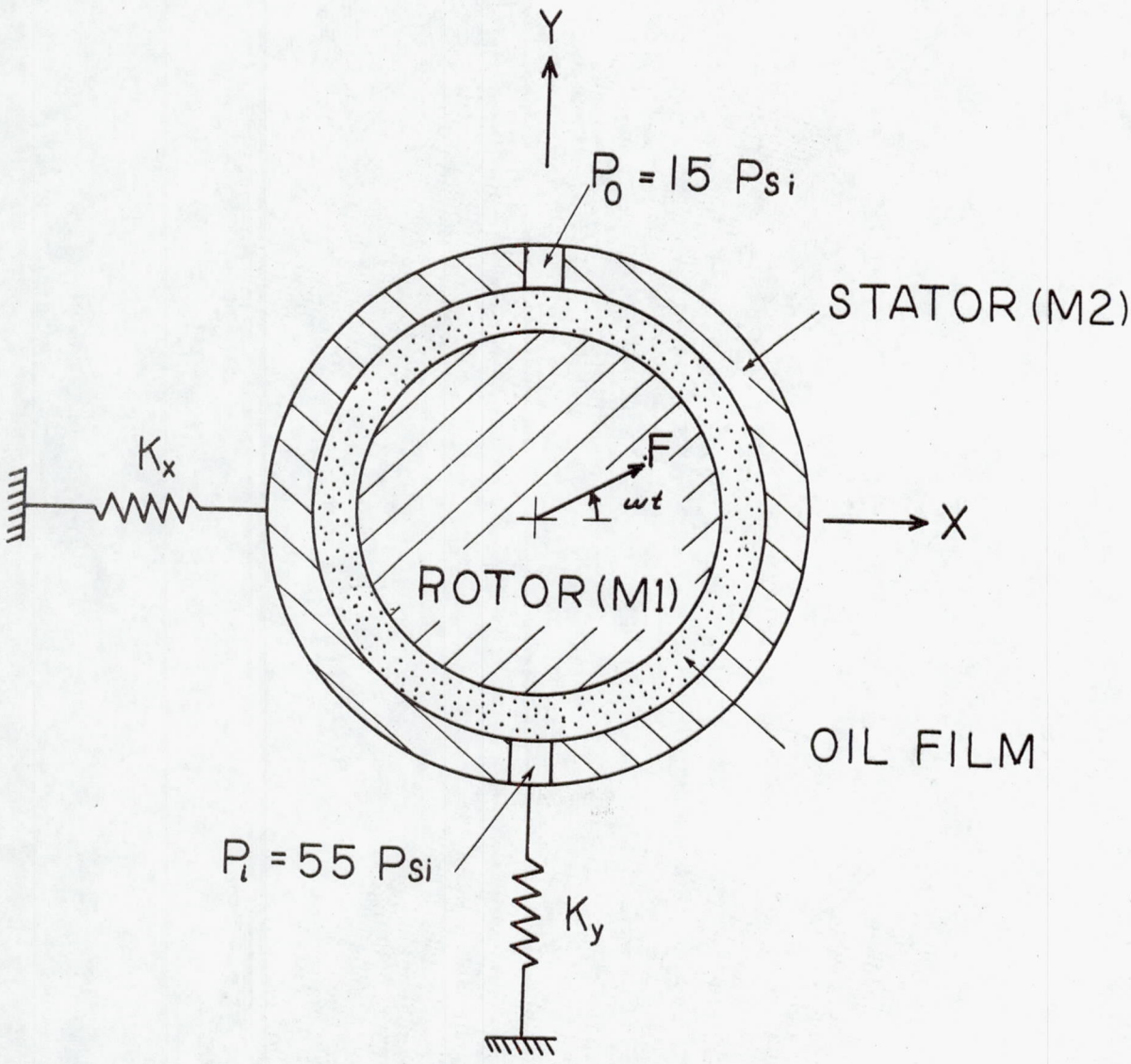

Figure 8 Simple 2-mass, 4-degree of freedom. Test case
(Same damper parameters as on page 23)

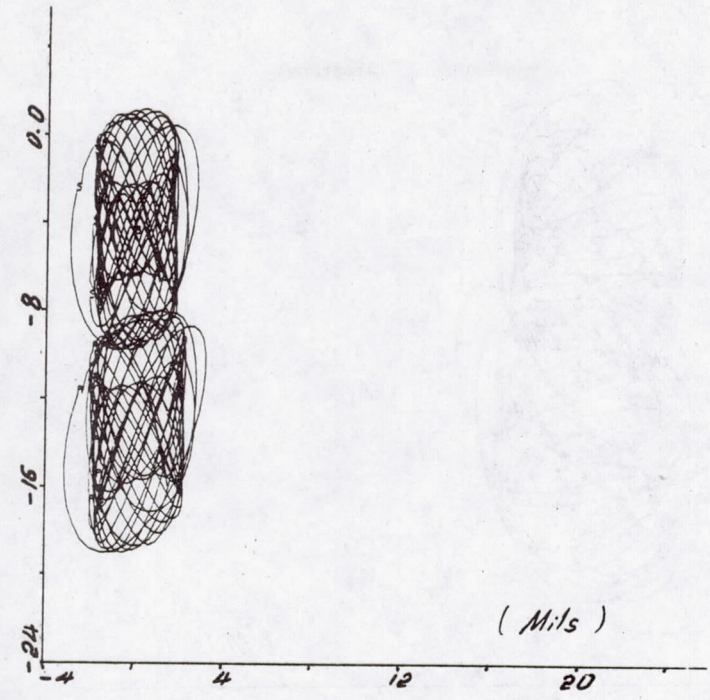

(a) Rotor and stator orbits

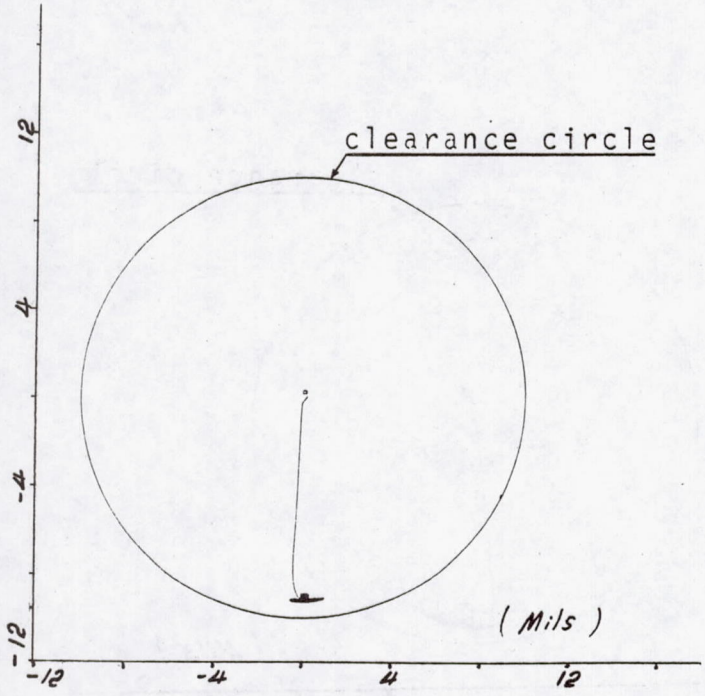

(b) Rotor orbit relative to stator (clearance circle shown)

Fig.9 Nonlinear dynamic transient of simple 4 DOE system(See Fig.8) $|F|$=100 lbs, ω=150 rad/sec, M1=M2=500 lbs, Kx=Ky=116000 lbs/in.

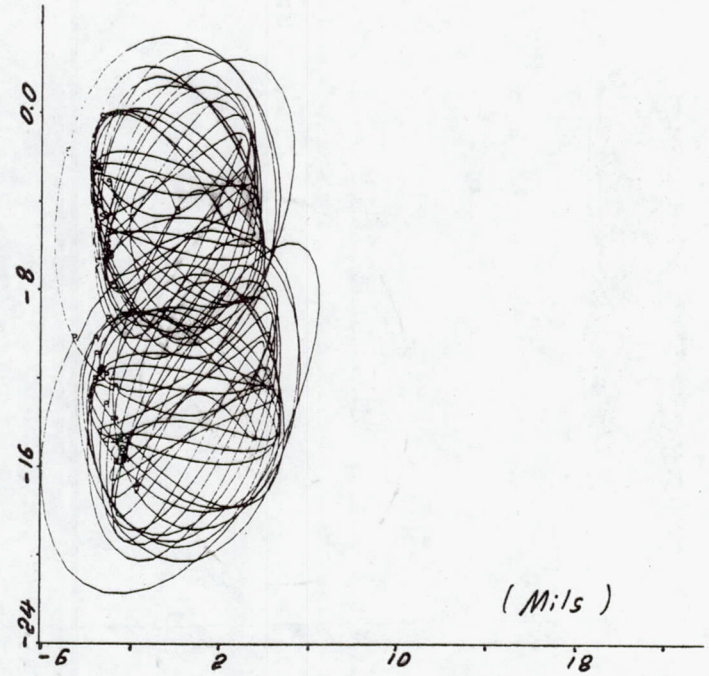

(a) Rotor and stator orbits

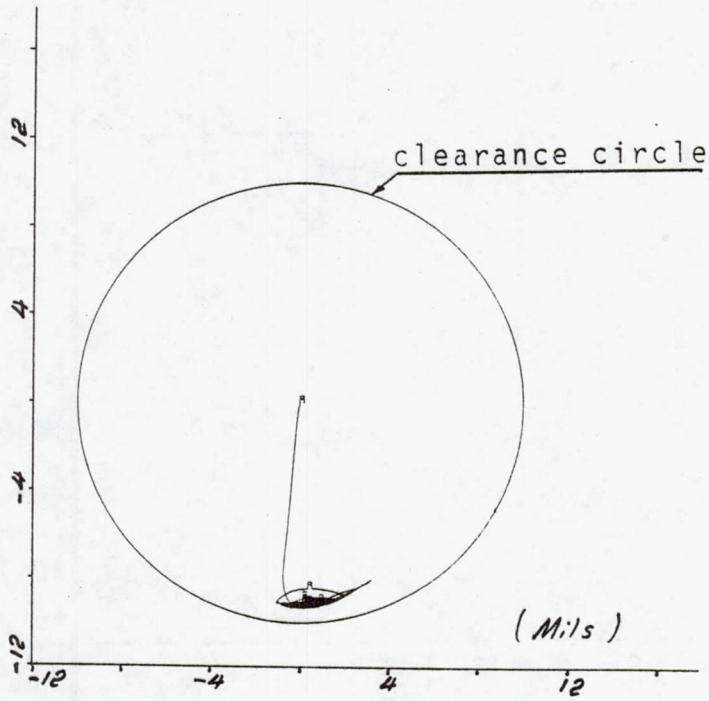

(b) Rotor orbit relative to stator (clearance circle shown)

Fig.10 Nonlinear dynamic transient of simple 4 DOE system(See Fig.8) $|F|$=200 lbs, ω=150 rad/sec, M1=M2=500 lbs, Kx=Ky=116000 lbs/in.

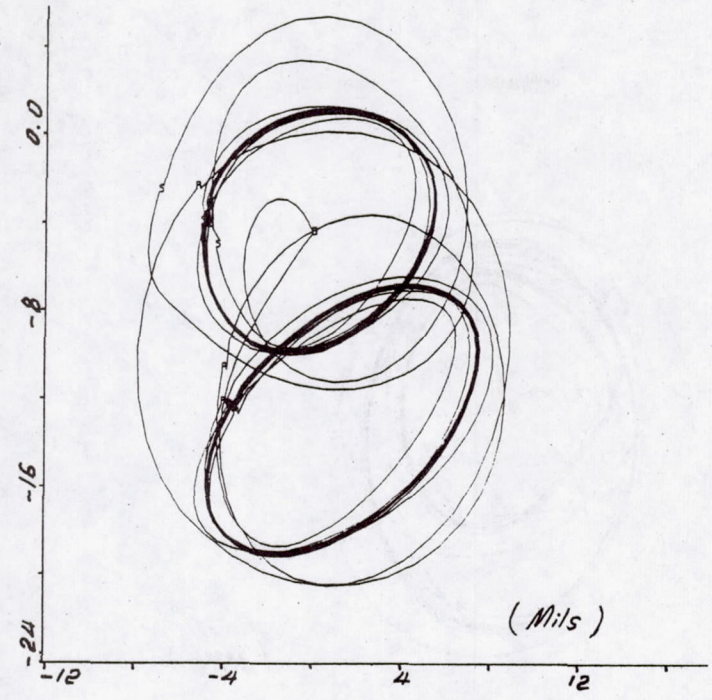

(a) Rotor and stator orbits

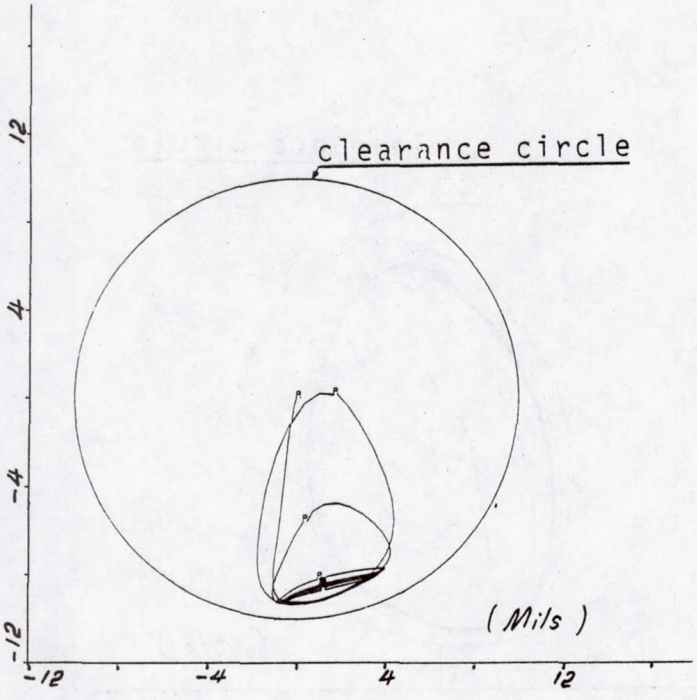

(b) Rotor orbit relative to stator (clearance circle shown)

Fig.11 Nonlinear dynamic transient of simple 4 DOE system(See.Fig.8) $|F|$=300 lbs, ω=150 rad/sec, M1=M2=500 lbs, Kx=Ky=116000 lbs/in.

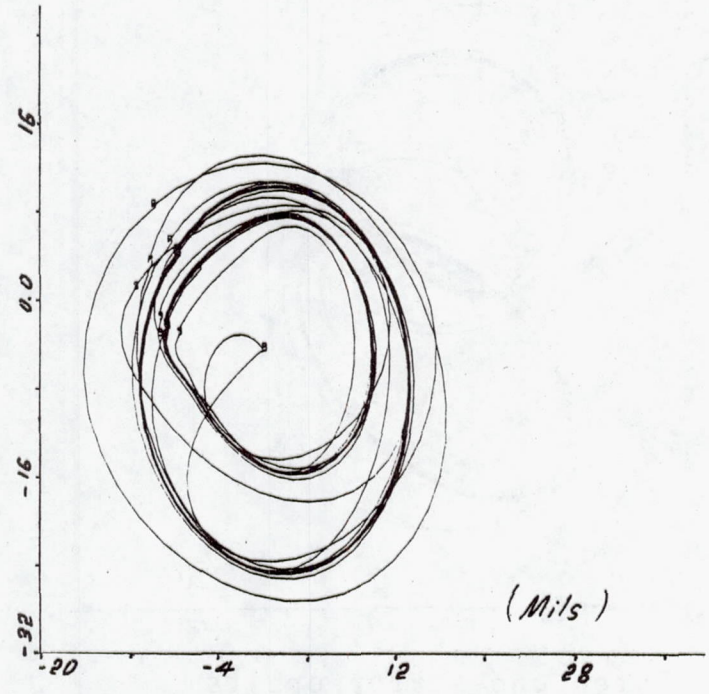

(a) Rotor and stator orbits

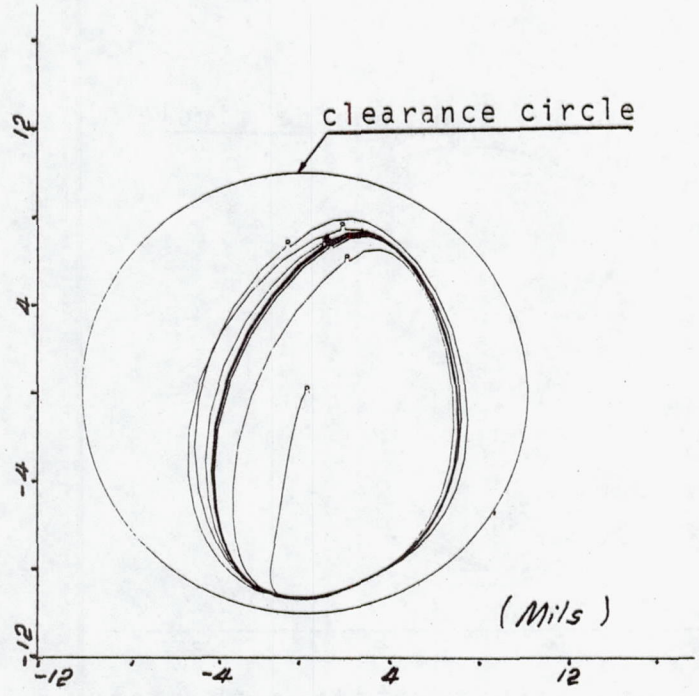

(b) Rotor orbit relative to stator (clearance circle shown)

Fig.12 Nonlinear dynamic transient of simple 4 DOE system(See Fig.8) $|F|$=500 lbs, ω=150 rad/sec, M1=M2=500 lbs, Kx=Ky=116000 lbs/in.

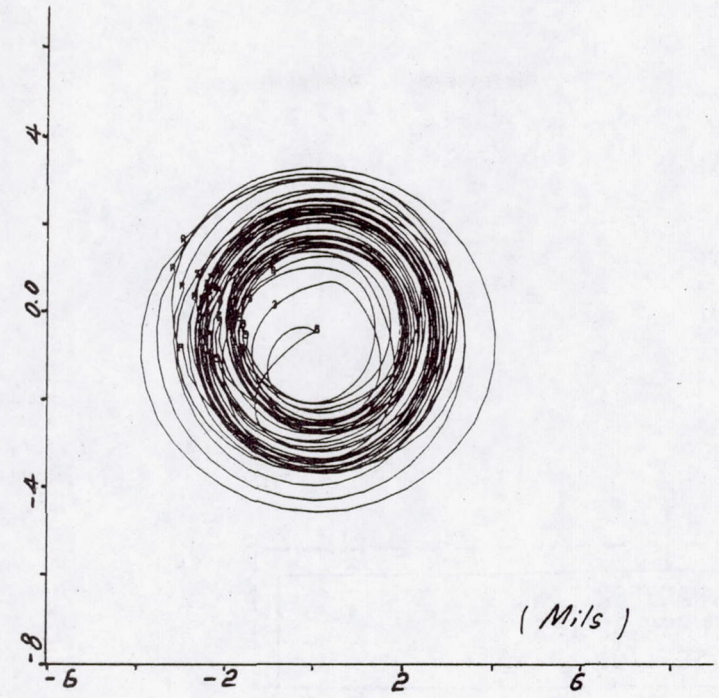

(a) Rotor and stator orbits

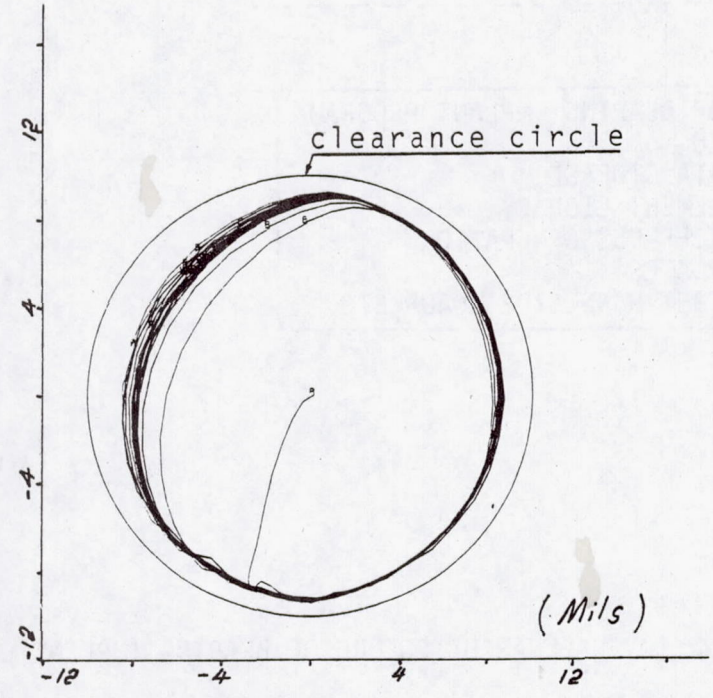

(b) Rotor orbit relative to stator
(clearance circle shown)

Fig.13 Nonlinear dynamic transient of simple 4 DOE system(See.Fig.8)
$|F|$=1000 lbs, ω=150 rad/sec, M1=M2=500 lbs, Kx=Ky=116000 lbs/in.

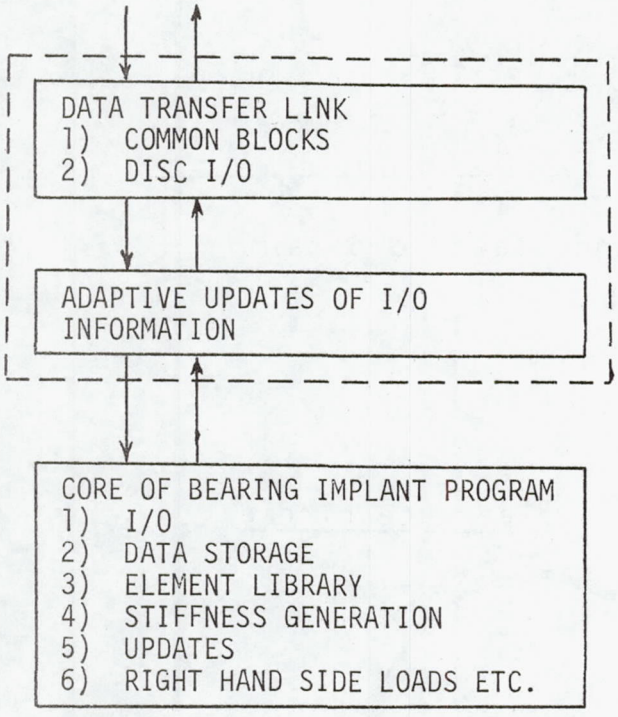

FIG. 14 (OVERALL ARCHITECTURE OF BEARING IMPLENT CODE)

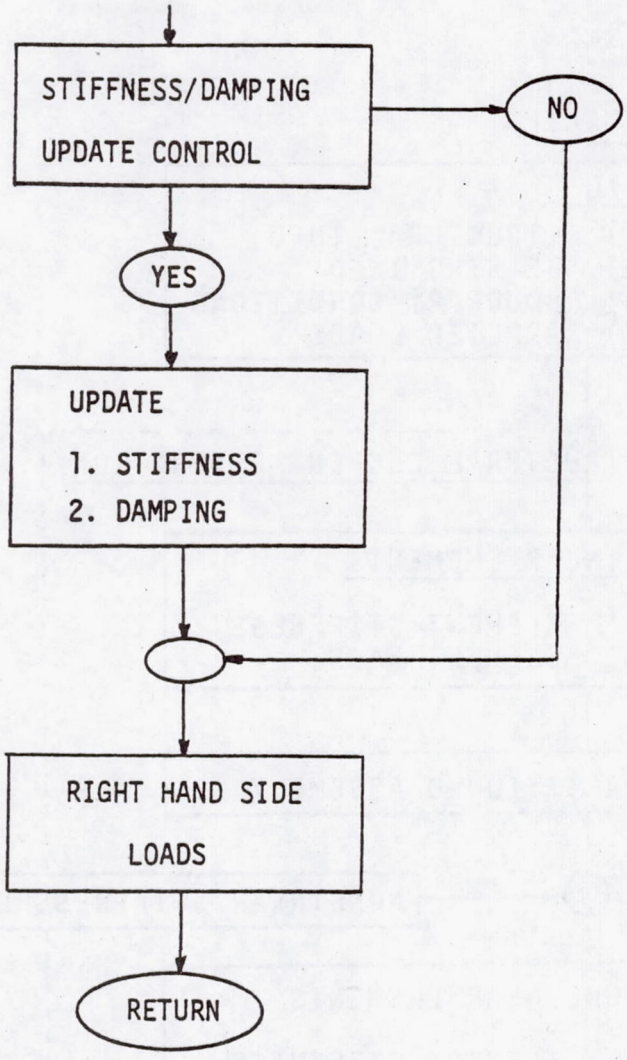

Fig. 15 ARCHITECTURE OF CORE PROGRAM OF "BEARING ELEMENT" IMPLANT

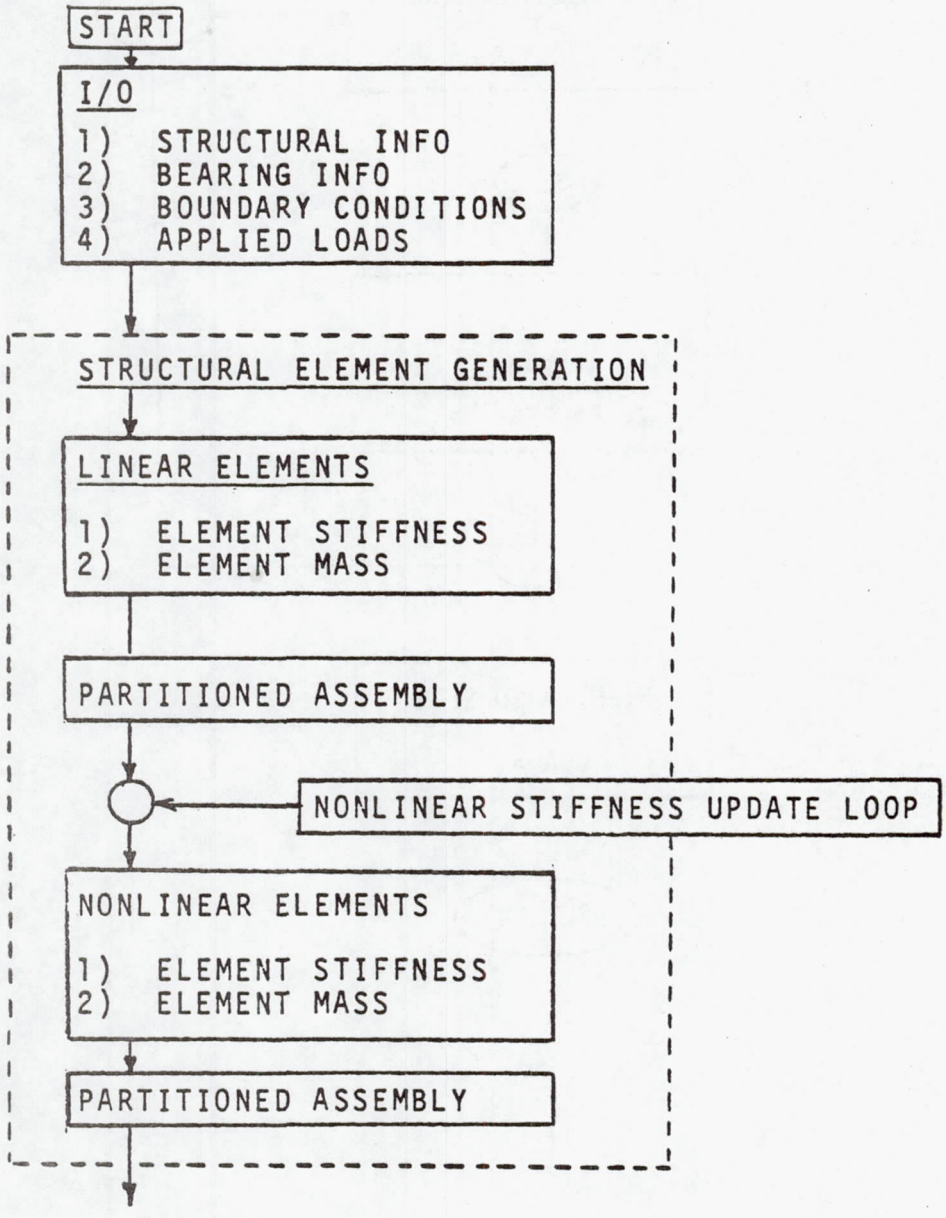

FIG. 16 (OVERALL FE CODE ARCHITECTURE)

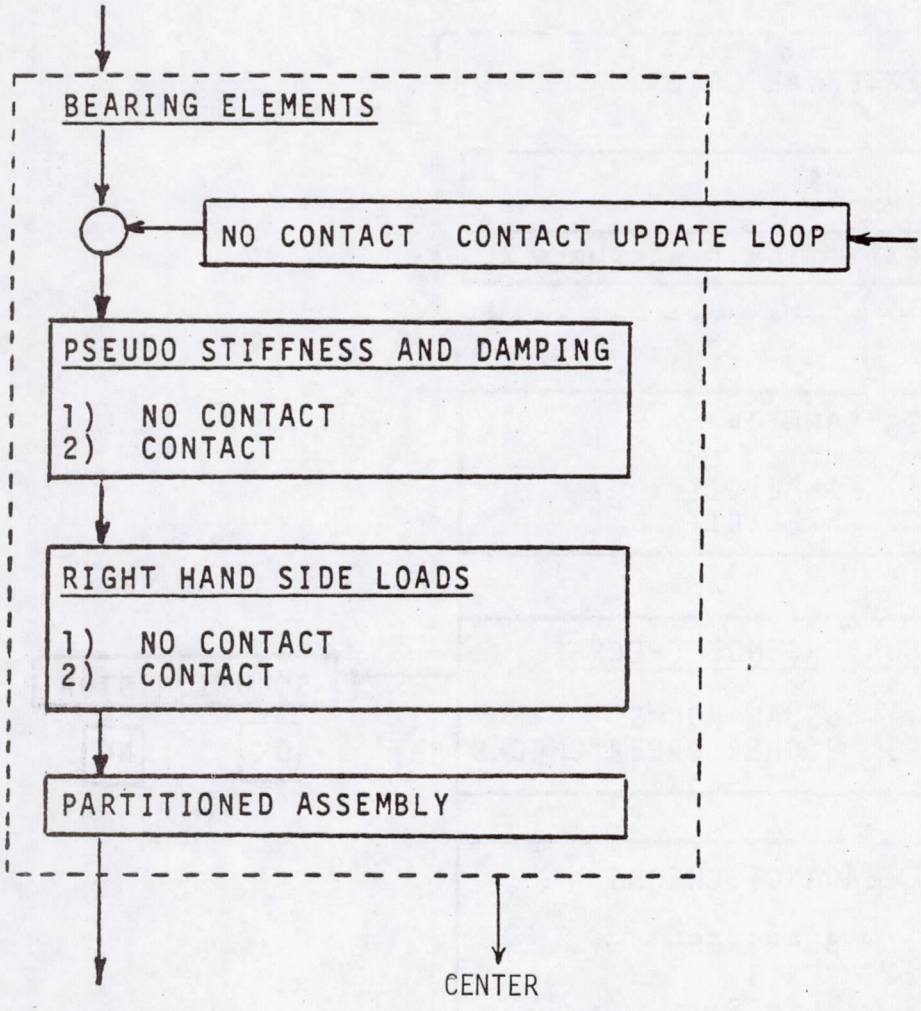
BEARING ELEMENTS
NO CONTACT
CONTACT UPDATE LOOP
PSEUDO STIFFNESS AND DAMPING
1) NO CONTACT
2) CONTACT
RIGHT HAND SIDE LOADS
1) NO CONTACT
2) CONTACT
PARTITIONED ASSEMBLY
CENTER

FIG.16 (CONT'D)

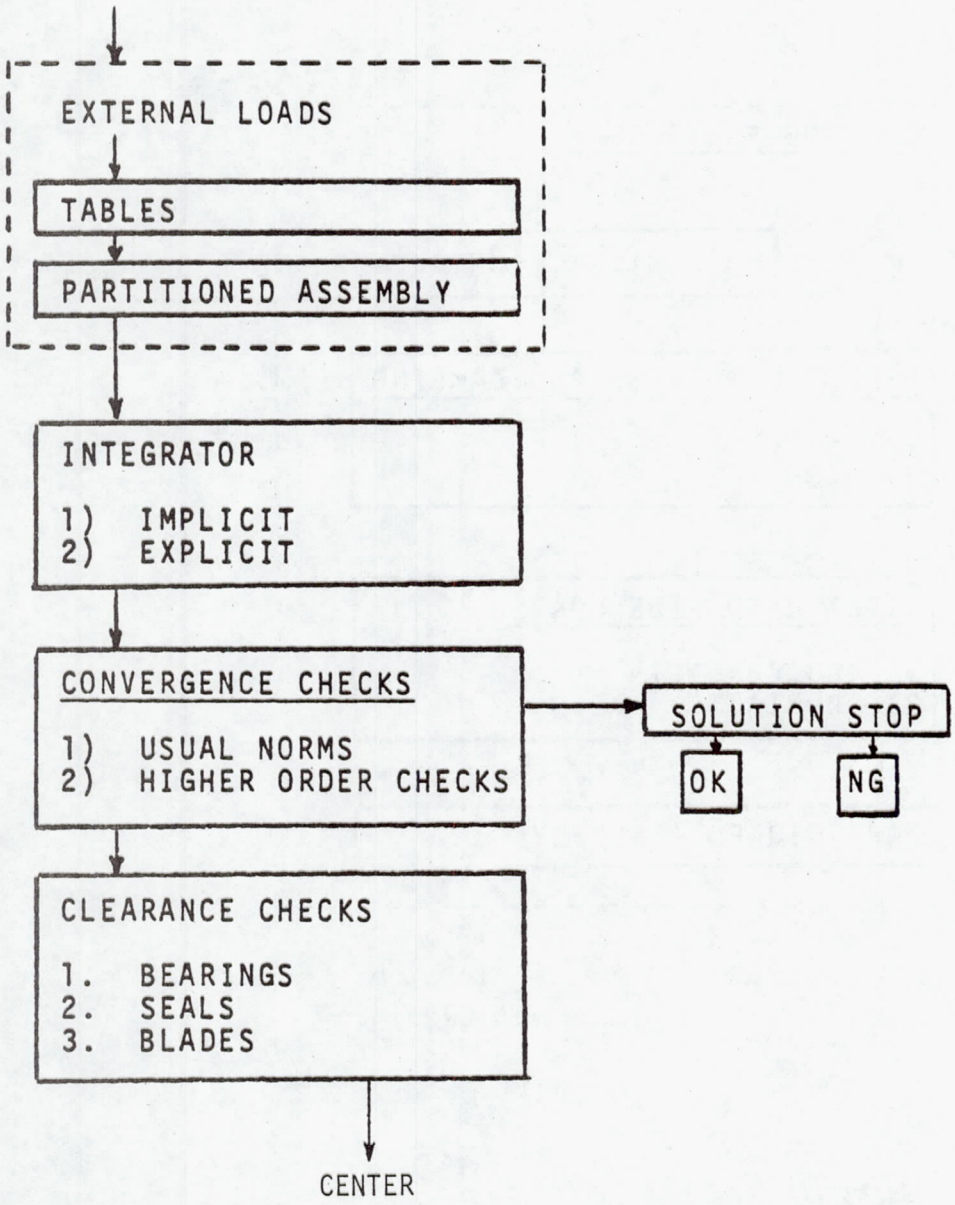
EXTERNAL LOADS
TABLES
PARTITIONED ASSEMBLY
INTEGRATOR
1) IMPLICIT
2) EXPLICIT
CONVERGENCE CHECKS
1) USUAL NORMS
2) HIGHER ORDER CHECKS
SOLUTION STOP
OK
NG
CLEARANCE CHECKS
1. BEARINGS
2. SEALS
3. BLADES
CENTER

FIG. 16 (CONT'D)

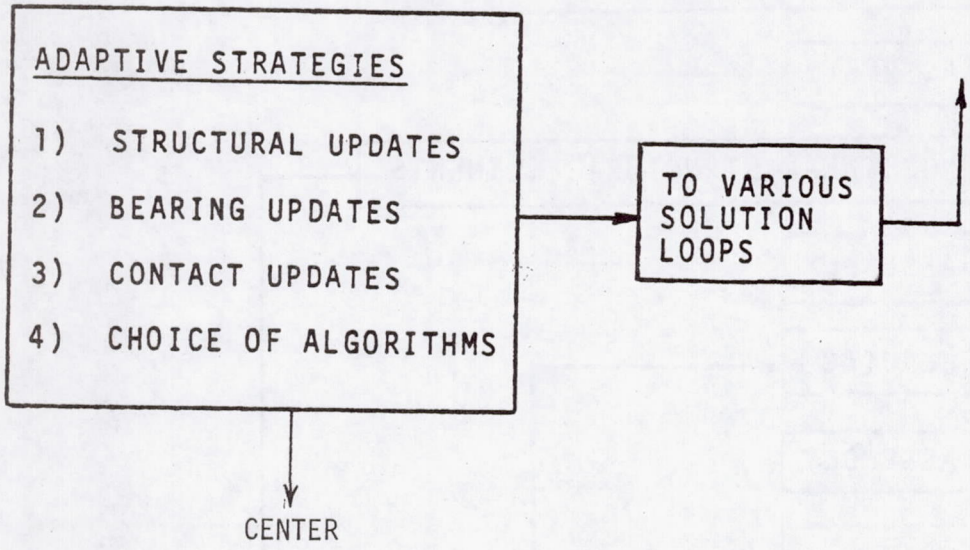
ADAPTIVE STRATEGIES
1) STRUCTURAL UPDATES
2) BEARING UPDATES
3) CONTACT UPDATES
4) CHOICE OF ALGORITHMS
TO VARIOUS SOLUTION LOOPS
CENTER

FIG. 16 (CONT'D)

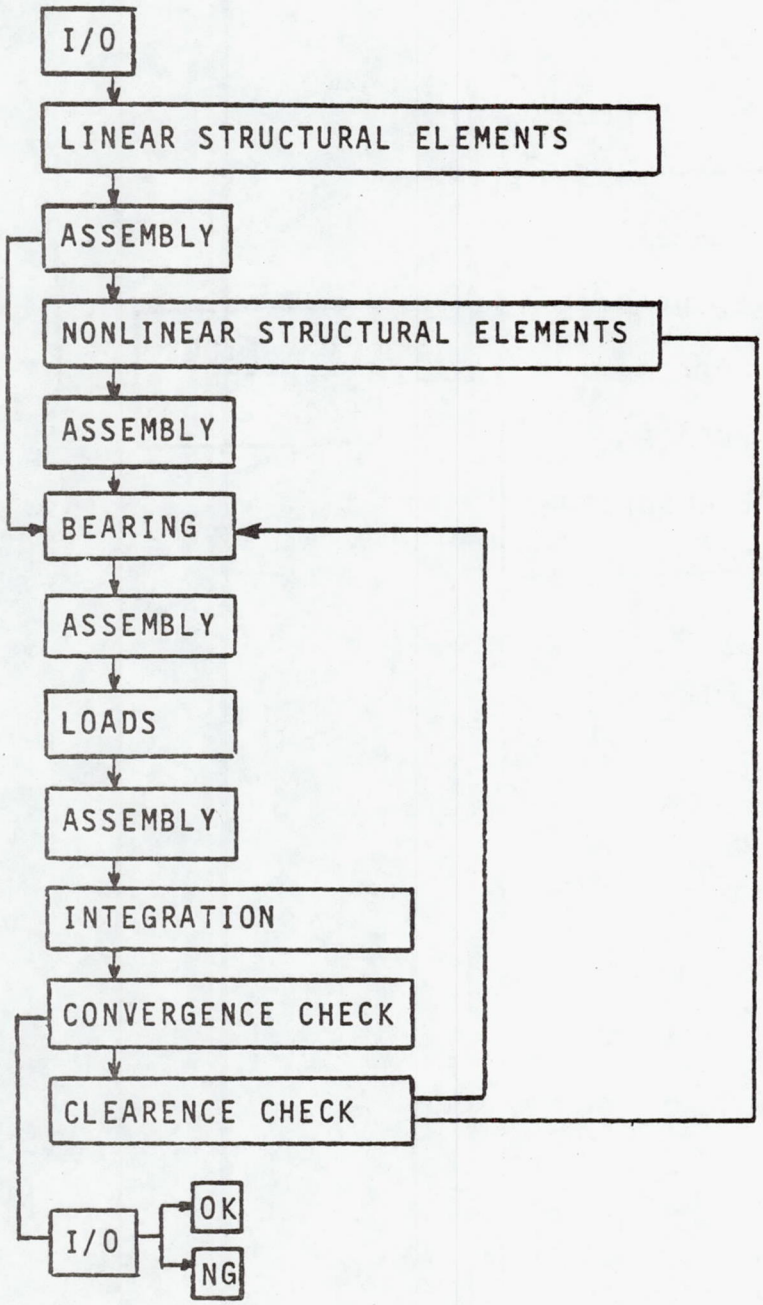

Fig. 17 (OVERALL PROGRAM FLOW)

DISTRIBUTION LIST FOR TOPICAL REPORT

NASA CR-165214

FINITE ELEMENT FOR ROTOR/STATOR INTERACTIVE FORCES IN GENERAL ENGINE DYNAMICS SIMULATION, PART I: DEVELOPMENT OF BEARING DAMPER ELEMENT

GRANT NSG-3283

	Mail Stop	Copies
NASA Lewis Research Center 21000 Brookpark Road Cleveland, OH 44135		
Attn: Contracting Officer	500-312	1
Technical Report Control Officer	5-5	1
Technology Utilization Office	3-16	1
AFSC Liaison Office	501-3	1
S&MT Division Contract File	49-6	2
Library	60-3	1
L. Berke	49-6	1
R. H. Johns	49-6	1
L. J. Kiraly	49-6	1
C. C. Chamis	49-6	7
M. S. Hirschbein	49-6	1
J. A. Ziemianski	49-6	1
W. J. Anderson	23-2	1
L. P. Ludwig	23-2	1
D. P. Fleming	23-2	1
A. F. Kascak	23-2	1
G. V. Brown	49-6	1
M. H. Tang	49-6	1
J. D. McAleese	49-6	1
National Aeronautics & Space Administration Washington, DC 20546		
Attn: NHS-22/Library		1
RTM-6/L. A. Harris		1
RTM-6/D. J. Weidman		1
NASA-Ames Research Center Moffett Field, CA 94035		
Attn: Library	202-3	1
NASA-Goddard Space Flight Center Greenbelt, MD 20771		
Attn: 252/Library		1
NASA-John F. Kennedy Space Center Kennedy Space Center, FL 32931		
Attn: Library	AD-CSO-1	1
NASA Langley Research Center Hampton, VA 23665		
Attn: Library	185	1
M. F. Card	244	1
M. M. Mikulas	190	1

	Mail Stop	Copies
NASA-Lyndon B. Johnson Space Center Houston, TX 77001 Attn: JM6/Library		1
NASA-George C. Marshall Space Flight Center Marshall Space Flight Center, AL 35812 Attn: AS61/Library		1
Jet Propulsion Laboratory 4800 Oak Grove Drive Pasadena, CA 91103 Attn: Library B. Wada R. Levi		1 1 1
NASA S&T Information Facility P.O. Box 8757 Baltimore-Washington Int. Airport, MD 21240 Attn: Acquisition Department		10
Air Force Aeronautical Propulsion Laboratory Wright Patterson AFB, OH 45433 Attn: Z. Gershon E. Bailey		1 1
Air Force Systems Command Aeronautical Systems Division Wright-Patterson AFB, OH 45433 Attn: Library C. W. Cowie J. McBane		1 1 1
Aerospace Corportion 2400 E. El Segundo Blvd. Los Angeles, CA 90045 Attn: Library-Documents		1
Air Force Office of Scientific Research Washington, DC 20333 Attn: A. K. Amos		1
Department of the Army U.S. Army Material Command Washington, DC 20315 Attn: AMCRD-RC		1
U.S. Army Ballistics Research Laboratory Aberdeen Proving Ground, MD 21005 Attn: Dr. Donald F. Haskell	DRXBR-BM	1
Mechanics Research Laboratory Army Materials & Mechanics Research Center Watertown, MA 02172 Attn: Dr. Donald W. Oplinger		1

	Mail Stop	Copies
U.S. Army Missile Command Redstone Scientific Information Center Redstone Arsenal, AL 35808 Attn: Document Section		1
AFFDL/FBE Wright-Patterson AFB, OH 45433 Attn: D. W. Smith		1
Commanding Officer U.S. Army Research Office (Durham) Box, CM, Duke Station Durham, NC 27706 Attn: Library		1
Bureau of Naval Weapons Department of the Navy Washington, DC 20360 Attn: RRRE-6		1
Commander U.S. Naval Ordnance Laboratory White Oak Silver Springs, MD 20910 Attn: Library		1
Director, Code 6180 U.S. Naval Research Laboratory Washington, DC 20390 Attn: Library		1
Denver Federal Center U.S. Bureau of Reclamation P.O. Box 25007 Denver, CO 80225 Attn: P. M. Lorenz		1
Naval Air Propulsion Test Center Aeronautical Engine Department Trenton, NJ 08628 Attn: Mr. James Salvino		1
Naval Air Propulsion Test Center Aeronautical Engine Department Trenton, NJ 08628 Attn: Mr. Robert DeLucia		1
Federal Aviation Administration Code ANE-214, Propulsion Section 12 New England Executive Park Burlington, MA 01803 Attn: Mr. Robert Berman		1

	Mail Stop	Copies
Federal Aviation Administration DOT Office of Aviation Safety, FOB 10A 800 Independence Ave., S.W. Washington, DC 20591 Attn: Mr. John H. Enders		1
FAA, ARD-520 2100 2nd Street, S.W. Washington, DC 20591 Attn: Commander John J. Shea		1
National Transportation Safety Board 800 Independence Ave., S.W. Washington, DC 20594 Attn: Mr. Edward P. Wizniak	TE-20	1
Arizona State University Department of Aerospace Engineering and Engineering Science Tempe, AZ 85281 Attn: H. D. Nelson		1
Rockwell International Corporation Los Angeles International Airport Los Angeles, CA 90009 Attn: Mr. Joseph Gausselin	D 422/402 AB71	1
Rensselaer Polytechnic Institute Troy, NY 12181 Attn: R. Loewy		1
Cleveland State University Department of Civil Engineering Cleveland, OH 44115 Attn: J. J. Tomko		1
M.I.T. Cambridge, MA 02139 Attn: K. Bathe T. H. Pian J. Mar E. A. Witmer J. Dugundji		1 1 1 1 1
University of Illinois at Chicago Circle Department of Materials Engineering Box 4348 Chicago, IL 60680 Attn: Dr. Robert L. Spilker		1

	Mail Stop	Copies
Detroit Diesel Allison General Motors Corporation Speed Code T3, Box 894 Indianapolis, IN 46206 Attn: Mr. William Springer Mr. J. Byrd		1 1
General Motors Corporation Warren, MI 48090 Attn: R. J. Trippet		1
AVCO Lycoming Division 550 South Main Street Stratford, CT 06497 Attn: Mr. Herbert Kaehler		1
Beech Aircraft Corporation, Plant 1 Wichita, KA 67201 Attn: Mr. M. K. O'Connor		1
Bell Aerospace P.O. Box 1 Buffalo, NY 14240 Attn: G. C. C. Smith		1
Boeing Aerospace Company Impact Mechanics Lab P.O. Box 3999 Seattle, WA 98124 Attn: Dr. R. J. Bristow		1
Boeing Commercial Airplane Company P.O. Box 3707 Seattle, WA 98124 Attn: Dr. Ralph B. McCormick		1
Boeing Commercial Airplane Company P.O. Box 3707 Seattle, WA 98124 Attn: Mr. David T. Powell	73-01	1
Boeing Commercial Airplane Company P.O. Box 3707 Seattle, WA 98124 Attn: Dr. John H. Gerstle		1
Boeing Company Wichita, KA Attn: Mr. C. F. Tiffany		1

	Mail Stop	Copies
McDonnell Douglas Aircraft Corporation P.O. Box 516 Lambert Field, MO 63166 Attn: Library		1
Douglas Aircraft Company 3855 Lakewood Blvd. Long Beach, CA 90846 Attn: Mr. M. A. O'Connor, Jr.	36-41	1
Garrett AiResearch Manufacturing Co. 111 S. 34th Street P.O. Box 5217 Phoenix, AZ 85010 Attn: L. A. Matsch		1
General Dynamics P.O. Box 748 Fort Worth, TX 76101 Attn: Library		1
General Dynamics/Convair Aerospace P.O. Box 1128 San Diego, CA 92112 Attn: Library		1
General Electric Company Interstate 75, Bldg. 500 Cincinnati, OH 45215 Attn: Dr. L. Beitch Dr. M. Roberts Dr. V. Gallardo	 K221 K221 K221	 1 1
General Electric Company Aircraft Engine Group Lynn, MA 01902 Attn: Mr. Herbert Garten		1
Grumman Aircraft Engineering Corp. Bethpage, Long Island, NY 11714 Attn: Library H. A. Armen		1 1
IIT Research Institute Technology Center Chicago, IL 60616 Attn: Library		1
Lockheed California Company P.O. Box 551 Dept. 73-31, Bldg. 90, PL. A-1 Burbank, CA 91520 Attn: Mr. D. T. Pland		1

	Mail Stop	Copies
Lockheed California Company P.O. Box 551 Dept. 75-71, Bldg. 63, PL. A-1 Burbank, CA 91520 Attn: Mr. Jack E. Wignot		1
Northrop Space Laboratories 3401 West Broadway Hawthorne, CA 90250 Attn: Library		1
North American Rockwell, Inc. Rocketdyne Division 6633 Canoga Avenue Canoga Park, CA 91304 Attn: Library, Dept. 596-306		1
North American Rockwell, Inc. Space & Information Systems Division 12214 Lakewood Blvd. Downey, CA 90241 Attn: Library		1
Norton Company Industrial Ceramics Division Armore & Spectramic Products Worcester, MA 01606 Attn: Mr. George E. Buron		1
Norton Company 1 New Bond Street Industrial Ceramics Division Worcester, MA 01606 Attn: Mr. Paul B. Gardner		1
United Aircraft Corporation Pratt & Whitney Group Government Products Division P.O. Box B2691 West Palm Beach, FL 33402 Attn: Library R. A. Marmol		1 1
United Aircraft Corporation Pratt & Whitney Aircraft Group 400 Main Street East Hartford, CT 06108 Attn: Library R. Liss D. H. Hibner C. Platt		1 1 1 1

	Mail Stop	Copies
United Aircraft Corporation Hamilton Standard Division Windsor Locks, CT 06096 Attn: Dr. G. P. Towsend Dr. R. A. Cornell		1 1
Aeronautical Research Association of Princeton, Inc. P.O. Box 2229 Princeton, NJ 08540 Attn: Dr. Thomas McDonough		1
Republic Aviation Fairchild Hiller Corporation Farmington, Long Island, NY Attn: Library		1
Rohr Industries Foot of H Street Chula Vista, CA 92010 Attn: Mr. John Meaney		1
TWA.Inc. Kansas City International Airport P.O. Box 20126 Kansas City, MO 64195 Attn: Mr. John J. Morelli		1
Stevens Institute of Technology Castle Point Station Hoboken, NJ 07030 Attn: F. Sisto A. T. Chang		1 1
Mechanical Technologies Inc. Latham, NY Attn: M. S. Darlow		1
Shaker Research Corporation Northway 10, Executive Park Ballston Lake, NY 12019 Attn: L. Lagace		1
Lockheed Palo Alto Research Labs Palo Alto, CA 94304 Attn: B. O. Almroth		1
Lockheed Missiles and Space Company Huntsville Research & Engineering Center P.O. Box 1103 Huntsville, AL 18908 Attn: H. B. Shirley		1

	Mail Stop	Copies
MacNeal-Schwendler Corporation 7442 North Figueroa Street Los Angeles, CA 90041 Attn: R. H. MacNeal		1
MARC Analysis Research Corporation 260 Sheridan Avenue, Suite 314 Palo Alto, CA 94306 Attn: P. V. Marcel		1
United Technologies Research Center East Hartford, CT 06108 Attn: Dr. A. Dennis		1
Georgia Institute of Technology School of Civil Engineering Atlanta, GA 30332 Attn: S. N. Atluri		1
Georgia Institute of Technology 225 North Avenue Atlanta, GA 30332 Attn: G. J. Simitsis		1
Lawrence Livermore Laboratory P.O. Box 808, L-421 Livermore, CA 94550 Attn: M. L. Wilkins		1
Lehigh University Institute of Fracture and Solid Mechanics Bethlehem, PA 18015 Attn: G. T. McAllister		1
Materials Science Corporation 1777 Walton Road Blue Bell, PA 19422 Attn: W. B. Rosen		1
National Bureau of Standards Engineering Mechanics Section Washington, DC 20234 Attn: R. Mitchell		1
Purdue University School of Aeronautics & Astronautics West Lafayetee, IN 47907 Attn: C. T. Sun		1
University of Dayton Research Institute Dayton, OH 45409 Attn: F. K. Bogner		1

	Mail Stop	Copies
Texas A&M University Aerospace Engineering Department College Station, TX 77843		
Attn: W. E. Haisler		1
J. M. Vance		1
V. P. I. and State University Department of Engineering Mechanics Blacksburg, VA 24061		
Attn: R. H. Heller		1
University of Arizona College of Engineering Tucson, AZ 87521		
Attn: R. H. Gallagher		1
J. C. Heinrich		1
University of California Department of Civil Engineering Berkeley, CA 94720		
Attn: E. Wilson		1
University of Kansas School of Engineering Lawrence, KS 66045		
Attn: R. H. Dodds		1
University of Virginia School of Engineering & Applied Science Charlottesville, VA 22901		
Attn: E. J. Gunter		1